Atmospheric
Measurement
Techniques

Discussions

Open Access

EGU

1 **Dynamic Infrared Gas Analysis from Longleaf Pine Fuelbeds Burned in a Wind**

2 **Tunnel: Observation of Phenol in Pyrolysis and Combustion Phases**

3 Catherine A. Banach,[1] Olivia N. Williams,[1] Ashley M. Bradley,[1] Russell G. Tonkyn,[1]

4 Joey Chong,[2] David R. Weise,[2] Tanya L. Myers,[1] Timothy J. Johnson[1]*

5 [1]Pacific Northwest National Laboratory, Richland, WA USA

6 [2]USDA Forest Service, Pacific Southwest Research Station, Riverside, CA, USA

7 *Contact: Timothy J. Johnson, timothy.johnson@pnnl.gov

8

9 **0. Abstract**

10 Pyrolysis is the first step in a series of chemical and physical processes that produce flammable

11 organic gases from wildland fuels that can result in a wildland fire. We report results using a new

12 time-resolved Fourier transform infrared method that correlates the measured FTIR spectrum to

13 an infrared thermal image sequence enabling identification and quantification of gases within

14 different phases of the fire process. The flame from burning fuel beds composed of pine needles

15 (*Pinus palustris)* and mixtures of sparkleberry, fetterbush and inkberry plants was the natural heat

16 source for pyrolysis. Extractive gas samples were analyzed and identified in both static and

17 dynamic modes synchronized to thermal infrared imaging: A total of 29 gases were identified

18 including small alkanes, alkenes, aldehydes, nitrogen compounds and aromatics, most previously

19 measured by FTIR in wildland fires. This study presents one of the first identifications of phenol

20 associated with both pre-combustion and combustion phases, using ca. 1 Hz resolution.

21 Preliminary results indicate ~2.5x greater phenol emission from sparkleberry and inkberry

22 compared to fetterbush, with differing temporal profiles.

23 **Keywords**: Fourier transform infrared, time-resolved, biomass burning, pyrolysis, phenol,

24 benzene, naphthalene, Pinus palustris, Lyonia lucida, Ilex glabra, Vaccinium arboreum

25 **1. Introduction**

26 Wildland fire is an important component of many ecosystems and has been used by humans for

27 several thousand years (Crutzen and Goldammer, 1993; Pyne, 1997; Scott et al., 2014). Many

28 North American ecosystems have evolved as a result of persistent fire (Barbour and Billings,

29   2000). The importance of fire in pine forests worldwide including the southern U.S. is well-known

30   (Agee, 2000; Christensen, 2000). In the U.S., prescribed burning is used on approximately 8

31   million ha annually to accomplish a variety of forestry and agricultural objectives (Melvin, 2015);

32   the impact of smoke from these fires has been studied for over 50 years (Chi et al., 1979; Biswell,

33   1989; Ward and Hardy, 1991; Hardy et al., 2001;). In the southern U.S., forest management

34   objectives include hazardous fuel reduction, site preparation, improved wildlife habitat, insect and

35   disease control, enhanced appearance and perpetuation of fire dependent species and natural

36   communities (Carter and Foster, 2004; Waldrop and Goodrick, 2012). The U.S. Department of

37   Defense (DoD) uses prescribed burning on approximately 243,000 ha annually for many of these

38   objectives as well as maintenance of critical training areas (Cohen et al., 2014). Many land

39   managers rely on fire behavior models to calculate fire movement on the landscape, energy release,

40   smoke plume development, dispersion and content (Bytnerowicz et al., 2009, Paton-Walsh et al.

41   2014). However, few fire behavior models account for the plethora of chemical reactions involved

42   in the fire. The heat transfer processes that take place in the fire environment are also only coarsely

43   described. In order to improve the use of prescribed burning to accomplish refined objectives,

44   more detailed description and modeling of the physical and chemical processes in fire are needed

45   (Cohen et al., 2014).

46   The chemical phases of wildland fire, described as preheating, flaming, smoldering and glowing

47   (Ward, 2001) are understood in a chemical sense, but only to varying degrees: While the chemical

48   effluents of flaming and smoldering phases have been characterized for many ecosystems and fuel

49   types at different scales (Ward and Radke, 1993), the physics and chemistry of the preheating

50   (pyrolysis) phase, have fewer studies beyond the bench scale (e.g. Depew et al., 1972;

51   Dimitrakopoulos, 2001; Susott, 1982; Tihay, 2010). To improve fire application models and to

52   accomplish the desired fire effects and limit potential fugitive emissions, improved understanding

53   is thus needed for many fundamental processes, particularly for pyrolysis and ignition in

54   heterogeneous fuel beds of live and dead fuels that reflect the diversity of vegetation found

55   worldwide. (Guérette et al. 2018).

56   Prior to oxidative combustion, biomass thermally decomposes in a heated environment. To study

57   this decomposition, thermogravimetric analysis has been applied to a small set of plant species

58   deemed to represent major wildland fuel types (e.g. Burgan and Susott, 1991; Susott, 1982). Others

59 have determined caloric content of southern fuels which is related to the composition of pyrolysis

60 products. (Hough, 1969; Behm et al., 2004). However, most such prior work used dried, ground

61 fuel samples in either an inert or oxidizing environment subject to uniform heating and heat

62 transfer, (Kibet et al. 2012) thereby eliminating the effects of moisture and heat transfer which are

63 key fire behavior variables. While pyrolysis and combustion of wildland fuels is known to be a

64 complex process (Zhou and Mahalingam, 2001), they are often modeled using simple

65 approximations in the relevant computer codes using the dominant gases of H_2, CO, CO_2 and CH_4.

66 Heat transfer in a wildland setting is less efficient than in thermogravimetric analysis: The amount

67 and composition of pyrolyzed species produced depend strongly on heating rate and temperature

68 and typically consists of oxidized small-molecule gases such as CO, CO_2, or H_2O, as well as non-

69 oxidized or partially oxidized species such as H_2, CH_4, C_xH_y, $C_xH_yO_z$ as well as tars. The products

70 of primary pyrolysis may react in the gas phase at elevated temperatures (i.e., secondary pyrolysis),

71 which may affect the amount of tar remaining.

72 This work is part of a larger project to measure and model pyrolysis gases from common wildland

73 fuels found on DoD installations in the southern United States. (Weise et al. 2018). The project

74 includes bench-level, laboratory-scale and field plot burns; integrating the results of the field and

75 laboratory measurements with the modeling results to identify potential improvements that can

76 enhance our understanding of pyrolysis and ignition in wildland fuels. During the course of the

77 project Fourier transform infrared (FTIR) technology has been used on several occasions to non-

78 intrusively measure the composition and concentration of the pyrolysis gases. This includes

79 identifying the gases liberated by: i) heating single leaf samples from several common southern

80 fuels using different heating modes in a pyrolyzer and in a simple flat-flame burner system, (Amini

81 et al., 2019; Safdari et al., 2020) ii) heating shrubs in prescribed burns at Ft. Jackson, South

82 Carolina, (Scharko et al., 2019a, b) and iii) heating nursery plants with flames from longleaf pine

83 needle fuel beds inside a wind tunnel (Aminfar et al., 2019). In order to achieve the goal that the

84 results be applicable to prescribed burns, a key focus has been linking the bench scale, wind tunnel

85 and field data to the models using realistic values and identities for the pyrolysis gases. Chemical

86 analysis of the foliage and results of the bench scale tests so far suggest that describing wood

87 pyrolysis may not be suitable for foliage fuels (live and dead) (Jolly et al., 2012; Jolly et al., 2016;

88 Matt et al., 2020); to date pyrolysis and ignition of wildland fuels have typically been based on

89 results for only cellulose or wood (e.g. Varhegyi et al., 1994; Di Blasi, 2008). We have extended

90   the number of southern fuels examined under more realistic conditions (Amini et al., 2019; Safdari

91   et al., 2018) including bench-scale measurements of burning individual leaves of plants reported

92   in this paper. A subset of the bench-scale plant species has been burned in a small wind tunnel to

93   bridge from the bench-scale to pyrolysis measurements made in the field. The wind tunnel

94   measurements were set to emulate the larger scale experiments with FTIR instruments and canister

95   samples in 0.1 ha prescribed burns at Ft. Jackson in May 2018.

96   Flames in laboratory and field experiments tend to be turbulent in nature meaning there is

97   inevitably some cross-contamination of the pyrolysis gases with flame gases produced in the

98   combustion reactions. It is necessary to decouple the phases so as to better understand the discrete

99   pyrolysis and combustion processes. The same can also be said of the many studies conducted at

100   larger facilities such as the Fire Sciences Laboratory (FSL) in Montana, USA. The FSL has long

101   path length optical cell coupled to an FTIR (Yokelson et al., 1996, Burling et al., 2010), as well as

102   many other powerful analytical methods such as proton-transfer mass spectrometry (Christian et

103   al., 2004; Warneke et al., 2011; Yokelson et al., 2013). The FTIR and many other systems at the

104   Missoula FSL have made first detections for dozens of chemical species and pioneered the science

105   of biomass burning in many regards. But because the sampling platform is 4 m above the floor,

106   there is mixing of gases from different phases. The combustion and smoldering phases are typically

107   easier to differentiate, primarily via the intrinsic diagnostic of the modified combustion efficiency

108   (MCE, Ward and Hao, 1991) which is a measure that is not independent of the composition of

109   smoke (Weise et al 2020). The same ambiguity as to the nature of the phase of fire also applies to

110   extractive methods whereby a sampling device attempts to capture pre-combustion phase gases.

111   Such sampling systems, typically connected to a field canister are effective but are subject to

112   vagaries of sniffer gas inlet placement, i.e. proximity to the pyrolyzing plant. (Scharko et al.

113   2019a,b).

114   In this paper we describe use of an FTIR with a dynamic probe to temporally isolate, identify and

115   quantify some of the early-stage/pyrolysis gases from burns at a mid-scale laboratory facility.

116   During three measurement episodes, experiments were conducted at the Riverside Fire Lab (RFL)

117   in a wind tunnel using fuel beds composed of longleaf pine needles and the live plants inkberry

118   (*Ilex glabra* (L.) A. Gray), fetterbush (*Lyonia lucida* (Lam.) K. Koch), sparkleberry (*Vaccinium*

119   *arboreum* L.) and blueberry (*V. darrowii* Camp). Multiple methods were used such as quantum-

120   cascade lasers (Phillips et al., 2020), gas chromatography-mass spectrometry as well as FTIR with

121   the overall objectives of: i) using careful chemometric extraction from the acquired data to see

122   what pyrolysis species can be identified by the techniques; ii) using the various methods to

123   determine the degree of oxidation or combustion, i.e. pyrolysis characterization; iii) making first

124   attempts to quantify the rates of evolution of pyrolysis products for certain plant species; and

125   ideally; iv) determining if differences exist between the pyrolysis emissions / temporal profiles for

126   different plant species. We take advantage of the time-resolved capabilities, as well as high

127   resolution specificity offered by IR spectroscopy and couple these to the flame/solid fuel

128   temperature diagnostics of an IR camera to analyze the emissions from a subset of 21 RFL burns.

129   ## 2. Experimental

130   *2.1 Wind Tunnel and Experimental Configuration*

131   During November 2017, February 2018 and November 2018 a total of 88 laboratory scale burns

132   were conducted at the USDA Forest Service Pacific Southwest Research Station in Riverside,

133   California. The laboratory includes a wind tunnel ca. 3 m long and 1 m wide which was set up to

134   simulate a forest floor of litter and live plants. Fuel beds composed of 1 kg of dry longleaf pine

135   needles and various combinations of fetterbush, sparkleberry, blueberry and inkberry (Fig. 1a)

136   were burned under either "no wind" or 1 m s^{-1} conditions. Fuel moisture content and mass loading,

137   ambient temperature and relative humidity in the tunnel were varied between experiments; fuel

138   beds were ignited with a line fire which propagated the length of the fuel bed as seen in Figure 1b.

139   Multiple analytical techniques were used to study the fire characteristics as well as the gas

140   effluents: thermocouples, Schmidt-Boelter flux sensor, nadir thermal IR camera and background-

141   oriented Schlieren photography (Aminfar et al 2019) to estimate heat transfer / air flow around the

142   plants, canister samples analyzed by GC/FID, quantum cascade (QC) infrared laser spectroscopy,

143   (Phillips et al., 2020) as well as broadband Fourier transform infrared (FTIR) spectroscopy. A

144   schematic overview of the experimental setup is seen in Figure 1c.

145
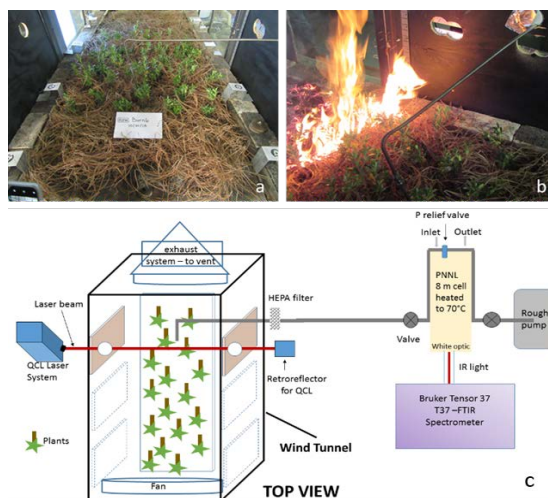
Figure 1. a) Overhead view of wind tunnel down its length with longleaf pine needles and interspersed
inkberry plants; b) flame front progressing down the wind tunnel with FTIR extraction tube visible; c)
cartoon (top view) of experimental layout with laser and FTIR systems.

Gas samples were pumped into the cell / FTIR instrument via a stainless steel probe mounted

above the plants (Fig. 1b). Gas from additional probes was pumped into canisters for offline

analysis using gas chromatography. Sixty-six or seventy-four live plants were distributed within

the longleaf pine needles in ceramic holders. Figure 1a shows the configuration of the fuel bed

with instrumentation for *in situ* analysis. Plant species were prepared on site and samples of dry

and live fuel were clipped to determine fuel moisture content prior to each burn set. The

experiments were set under varying fuel bed and environmental conditions. See Table 1 for the

conditions in the 21 experiments presented in this paper.

Table 1. Summary of burn schedule for November 2018 studies including burn number, date and time, fuel
description, acquisition method and resolution used for wind tunnel experiments under 1 m s^{-1} imposed air flow.
Geometric mean flame spread rate = 0.01 m s^{-1}. The FTIR acquisition methods are described in the text.

160

Atmospheric
Measurement
Techniques
Discussions

Burn number	Date (2018)	Local ignition time (PDT)	Local finish time (PDT)	Plant species	Acquistion method	Resolution (cm^{-1})
76	30-Oct	11:48:01	11:52:00	inkberry	static	0.6
77	30-Oct	14:19:10	14:23:37	fetterbush	dynamic	2.0
78	30-Oct	15:12:30	15:16:33	sparkleberry	static	0.6
79	30-Oct	16:17:00	16:21:10	inkberry	dynamic	2.0
80	31-Oct	9:32:00	9:35:45	sparkleberry	static	0.6
81	31-Oct	10:35:00	10:38:52	fetterbush	dynamic	1.0
82	31-Oct	11:30:30	11:35:15	sparkleberry	static	0.6
83	31-Oct	13:19:00	13:22:58	inkberry	dynamic	1.0
84	31-Oct	14:12:15	14:16:30	fetterbush	static	0.6
85	31-Oct	15:30:30	15:34:24	fetterbush	dynamic	2.0
86	1-Nov	9:30:00	9:33:02	sparkleberry	dynamic	1.0
87	1-Nov	10:40:00	10:42:49	inkberry	dynamic	1.0
88	1-Nov	11:40:00	11:42:59	fetterbush	static	0.6
89	1-Nov	13:35:00	13:38:48	inkberry	static	0.6
90	1-Nov	14:45:00	14:49:47	sparkleberry	static	0.6
92	2-Nov	9:30:00	9:34:05	inkberry	dynamic	0.6
93	2-Nov	10:41:15	10:45:44	fetterbush	dynamic	1.0
94	2-Nov	11:28:15	11:32:28	sparkleberry	static	0.6
95	2-Nov	13:42:45	13:46:17	sparkleberry	static	0.6
97	2-Nov	15:38:38	15:41:40	sparkleberry	dynamic	0.6

161

Atmospheric
Measurement
Techniques
Discussions

162

2.2 Instrumentation

164 Gases were extracted from the burns via 3/8" stainless steel tubing, HEPA filtered to eliminate tar

165 and char contamination and pumped into an 8-meter White cell (Bruker A136, 2.2 liter volume)[1]

166 housed inside a Bruker Tensor 37 spectrometer (Figure 1c). The extractive probe was placed

167 directly above a plant as close as possible to the foliage. To prevent analyte/tar condensation, both

168 transfer tubing and the gas cell were heated to ~50 °C using heating tape/voltage regulator and a

169 cell heating shroud, respectively. A thermocouple was suspended into the White cell to record the

170 gas temperature for subsequent spectral analysis, with pressure gauge mounted atop the cell. Prior

171 to data collection, the White cell was aligned using the FTIR's Ge/CaF$_2$ beamsplitter and W-lamp

172 source. Once aligned, these were replaced with a Ge/KBr beamsplitter and mid-IR globar source,

173 along with a mercury cadmium telluride detector, configuring the Tensor 37 to record spectral data

174 from 7500 to 500 cm^{-1}.

175 The FTIR system was tested for leaks, followed by a gas cell path length calibration using purified

176 isopropyl alcohol (IPA - Sigma Aldrich 99.5%). Ten spectra with IPA pressures between 0.6 and

177 10.5 Torr were recorded to 0.1 Torr using an MKS KF15 pressure transducer. The integrated area

178 of the 3515-3290 cm^{-1} spectral domain (Bruker OPUS 5.5 software) along with recorded

179 temperatures and pressures were used to create a Beer-Lambert plot (Scharko et al. 2019a). Using

180 the integrals from the ten recorded spectra the cell path length was determined to be 6.5 ± 0.2 m.

181 Wavelength calibration of the infrared data was achieved after the fact using a series of 30 water

182 rotational-vibrational lines from the PNNL gas-phase database. (Sharpe et al. 2002; Williams et

183 al., 2013). FTIR interferograms were acquired using double-sided, forward-backward acquisition;

184 these were apodized using a Blackman-Harris 3-Term function and phase corrected with Mertz's

185 method prior to Fourier transformation.

2.3 Infrared spectral acquisition

187 Two data acquisition modes were used to analyze the burn gases: an extractive (or static) mode

188 and a dynamic mode. In the extractive mode the gas flowing through the White cell was isolated;

189 the inlet/outlet valves were simultaneously closed such that the emitted gases were isolated in the

---

[1] The use of trade or firm names in this publication is for reader information and does not imply endorsement by the U.S. Department of Agriculture of any product or service.

Atmospheric
Measurement
Techniques
Discussions

Open Access

EGU

190   cell at a desired pressure (ca. 740-700 Torr for high pressures, and 430-400 Torr for lower pressure

191   measurements). The valves were closed just prior to the flame front reaching the probe, attempting

192   to capture pre-combustion phases including evaporation and pyrolysis. The goal of the extractive

193   mode was to obtain a higher fidelity "snapshot" for a given point in time of the burn; more data

194   were averaged longer at higher spectral resolution allowing for detection of more gaseous species

195   with higher sensitivity. (Scharko et al., 2019a). The dynamic mode measurements had fewer scans

196   at lower resolution to capture changing chemical identities/composition corresponding to different

197   fire phases (pyrolysis, flaming combustion, smoldering combustion), achieving temporal

198   resolutions of the order of ca. 1 Hz.

199   Of the 21 burns, 10 were recorded using the static method. The static experiment spectra were

200   recorded using the full resolution of the spectrometer (0.6 cm^{-1}), a 2 mm Jacquinot stop and double

201   sided, forward-backward acquisition. Due to the higher resolution and lower light throughput,

202   acquisition time was extended by averaging multiple scans for a full 30 minutes, resulting in vastly

203   improved signal/noise ratios (SNR). For analysis of such complicated gas-phase mixtures, infrared

204   spectral resolutions of 1.0 cm^{-1} or better have been demonstrated to be advantageous (Burling et

205   al., 2010, Akagi et al., 2014, Scharko et al., 2019a). While one goal was to isolate gases to include

206   only the pyrolysis and pre-combustion phases, one vagary of the technique involved the timed

207   closing of the valves relative to arrival of the flame front approaching the inlet. If the valves were

208   shut too early, the captured emissions would consist of only (warmed) ambient gas before onset

209   of thermal degradation of the solid fuel, as opposed to the desired pyrolysis phase. Conversely, if

210   shut too late, flaming, or possibly even smoldering conditions would be sampled.

211   The second method was the dynamic mode whereby the OPUS software was used to continuously

212   collect interferograms throughout the duration of the burn, capturing the chemical compositions

213   associated with different phases, e.g. volatilization, heating, pyrolysis, flaming or smoldering

214   combustion. Fourier transformation of the interferograms occurred after the burns to yield faster

215   acquisition times. The dynamic acquisition mode was used in combination with thermal IR video

216   imaging recorded from above the flame bed to help synchronize spectral acquisition to the various

217   burn phases for a total of 11 burns. Instead of averaging for 30 minutes, the dynamic method

218   allowed for 40-80 continuous interferometer scans (differing on the duration of the burn), and

219   yielded a spectrum every 1.5 s for data taken at 1.0 cm^{-1} resolution, every 0.79 s for data at 2.0 cm^{-}

220   ^{1} resolution, and every 2.5 s for 0.6 cm^{-1} resolution spectra. Data acquisition began as the flame

Atmospheric
Measurement
Techniques
Discussions

221   front encroached upon the extractive probe and continued until the flame had passed. Due to the

222   faster acquisition rate these spectra are significantly noisier than the data collected using the

223   extractive method. To compare results from the static and dynamic modes, fires 87 and 89 will be

224   presented. The 2 m length fuel beds for both experiments 87 and 89 consisted of 1 kg longleaf pine

225   needles with interspersed inkberry plants.

226   For time synchronization it was necessary to quantify the time lag from the time the emissions

227   enter the extractive probe to midpoint in their flow through the White cell. A flow rate test was

228   thus conducted using freon gas, CFC-11 (trichlorofluoromethane) which is comparable in

229   molecular weight to the heavier gases detected by the FTIR. Figure 2 shows such a test of CFC-

230   11 being introduced with spectra recorded every 0.79 s using 2.0 cm^{-1} resolution. The time from

231   introduction of the freon at the extractive probe (t=0, scan 0) to first appearance in scan 4 (maroon

232   trace) was 3.2 seconds. The freon spectra had maximized at scan 6 (red trace) for a total Δ t = 4.8

233   s lag from the probe to the instrument. With this information, FTIR time stamped data were then

234   adjusted to reflect the 4.8 second time delay which was used when correlating the spectral data to

235   the visual and thermal IR video images.
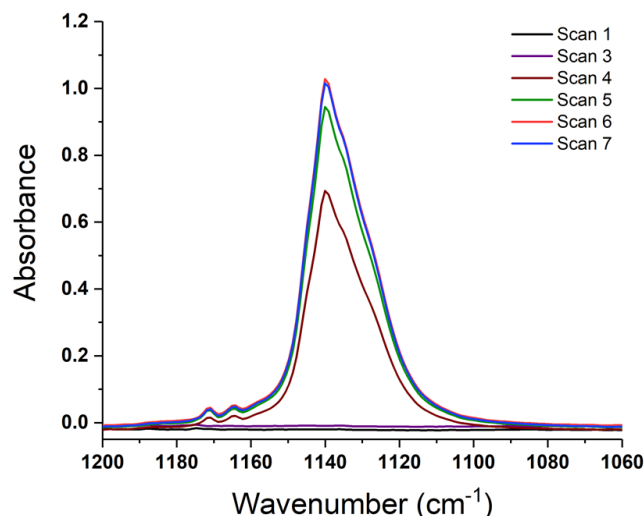
236
237   **Figure 2:** Dynamic spectra recording introduction of CFC-11 from extractive probe to gas cell. Scan 0 (not
238   shown) represents start of spectral acquisition/freon release near probe. Spectra produced every 0.79 s. First
239   observation of freon occurs with scan 4; maximum absorbance of CFC-11 and stabilization occurs at scan 6.

240   *2.4 Spectral Analysis*

241   A combination of software was used for the post-acquisition spectral analysis and confirmation of

242   the species observed during the campaign. The MALT5 software (Griffith, 2016) utilizing both

243   HITRAN line-by-line data (Gordon et al., 2017) as well as the PNNL 50 °C gas-phase reference

244   spectra (Kochanov, 2019; Johnson et al., 2006, 2010) as input libraries was used to identify and

245   quantify vapor-phase chemicals in the spectra. Spectra were compiled into parameter files and

246   analyzed by the MALT software using parameters including pressure, temperature, pathlength,

247   resolution, as well as estimated initial values for chemical mixing ratios. The software generates a

248   spectrum to simulate the measured spectrum, adjusting mixing ratios until the residual between

249   the simulated and measured spectra is minimized. To confirm the species were actually present,

250   each spectrum generated by MALT was input to OPUS and subtracted from the measured

251   spectrum; the target compound was purposefully omitted from the subtraction process to visually

252   inspect if the omitted compound was in fact present (see e.g. Figure 5).

3. Results and Discussion

254   *3.1 Analysis of Static Spectra*

255   Ten spectra were recorded from different burns using the static mode with the gas cell valves

256   closed simultaneously; gases were sampled prior to arrival of the flame front (Figure 1c). A total

257   of 29 compounds were detected and confirmed using MALT5 and OPUS 5.5. Along with CO,

258   CO_2 and nitrogen compounds, the gas-phase species are largely lightweight hydrocarbons (HCs),

259   volatile organic compounds (VOCs) and oxygenated volatile organic compounds (OVOCs). Table

260   2 provides a summary of all compounds observed during the static measurements and is broken

261   down into subcategories of chemical classes by rows labeled a-e, with ambient gases such as CO

262   and CO_2 in group a, alkanes and alkenes in group b, alcohols, aldehydes and carboxylic acids in

263   group c, aromatic species in group d, and N-bearing compounds in group e. The benefits of the *in*

264   *situ* laboratory static measurements were controlled gas sample collection with FTIR analysis and

265   longer scan times for increased SNRs at higher spectral resolution. Valves were shut before the

266   flame front arrived allowing for minimal mixing of air and flame gases near the extractive probe.

267   In this manner the targeted pyrolysis phase was likely to be sampled with a greater mole fraction

268   rather than that of the combustion phase. The gases listed in Table 2 have previously been

269   observed in smoke in either field or laboratory settings, and some have been linked to pyrolysis

270   (Scharko, 2019a,b; Burling et al., 2010, 2011; Christian et al., 2003, 2004; Gilman et al., 2015;

271   Goode et al., 1999, 2000; Hatch et al., 2017; Selimovic et al., 2018; Stockwell et al., 2014;

272   Yokelson et al., 1996, 1997; Akagi et al., 2013, 2014; Alves et al., 2010; Hurst et al., 1994a, b;

Atmospheric
Measurement
Techniques
Discussions

Open Access
EGU

273 Karl et al., 2007; Paton-Walsh et al., 2010). Compounds associated with the pyrolysis phase and

274 observed in several of the static measurements include acetic acid, ethene (C_2H_4), allene, 1,3-

275 butadiene, acetaldehyde, formic acid, formaldehyde, acrolein, benzene, furan, furaldehyde,

276 naphthalene and phenol.

277 As seen in Table 2, ammonia gas (NH_3) was also detected at fairly low mixing ratios in the

278 laboratory scale experiments, which had previously not been detected in the Ft. Jackson field

279 study: The lack of NH_3 detection in those studies was ascribed to the known adsorptivity of the

280 compound as it may have adhered to either the transfer canister walls, the extractive probe, or the

281 White Cell, all at ambient temperatures as used in those studies (Scharko et al., 2019; Roscioli et

282 al., 2015; Stockwell et al, 2014; Yokelson et al., 2003; Neuman et al., 1999). Adhesion losses

283 were minimized in the present experiments by a) measuring the gas parcel directly without storage

284 and b) heating transfer lines and gas cell to ~55 °C.

285 **Table 2.** Mixing ratio of chemicals from spectra collected using the static acquisition method. Burns are labeled
286 by number and plant species. Compound mixing ratios are reported in ppm (with the exception of H_2O and CO_2
287 reported as percents) and categorized by (a) background ambient compounds, (b) simple hydrocarbons, (c)
288 oxygenated organic compounds, (d) aromatics, and (e) N-bearing species.

		Burn 76	Burn 78	Burn 80	Burn 82	Burn 84	Burn 88	Burn 89	Burn 90	Burn 94	Burn 95
		inkberry	sparkleberry	sparkleberry	sparkleberry	fetterbush	fetterbush	inkberry	sparkleberry	sparkleberry	sparkleberry
a	% H_2O	1.24	1.05	3.23	2.03	3.54	3.08	3.46	1.82	6.21	4.10
	% CO_2	0.06	0.09	2.06	0.48	1.51	2.06	1.36	0.34	4.60	2.08
	CO	1.45	3.90	808	192	1089	1057	391	160	7506	2651
	N_2O	0.35	0.34	1.21	0.50	1.28	1.79	0.44	0.41	3.22	1.78
b	CH_4	2.27	2.21	45.3	10.7	54.5	50.3	15.4	11.3	682	198
	C_2H_2	0.01	0.06	23.8	4.52	23.4	23.2	8.82	5.62	351	96.5
	C_2H_4	0.07	0.05	29.3	7.05	39.9	39.3	9.66	6.52	452	133
	C_2H_6			0.83			2.76		4.00E-04	24.2	6.29
	C_3H_6			4.02	0.99	5.55	5.48	0.75	0.77	61.3	18.1
	allene	0.17		0.64	0.29	1.12	1.21	0.25	0.12	8.69	2.30
	1,3-butadiene			1.63	0.37	1.98	2.07	0.26	0.43	28.1	7.57
	isobutene			0.75		0.74	0.52			3.16	1.07
	isoprene			1.78	0.39	1.72	1.43	0.31	0.32	11.7	4.22
c	CH_3OH	0.89	0.24	6.81	1.53	6.92	9.44	1.66	0.93	42.3	18.0
	C_2H_5OH	1.37									
	acetic acid	0.07		5.93	3.55	13.4	13.8	11.0	2.49	13.4	9.62
	formic acid			15.9	5.14	32.35	35.3	9.20	3.64	130	73.6
	acetaldehyde			5.87	1.69	7.62	8.65	1.51	0.94	73.6	22.6
	acrolein			2.59	1.29	3.99	4.35	0.98	0.00	26.0	9.53
	crotonalehyde			1.51	0.54			0.73	0.17	9.97	5.64
	formaldehyde		0.08	13.6	4.31	21.3	22.5	5.41	3.33	114	52.8
d	benzene			4.08	2.23	5.19	4.24	1.93	1.48	61.3	18.6
	furan			0.75		0.39	0.54			3.07	1.16
	furfural			0.65	0.06				0.13	3.34	1.24
	naphthalene			4.48	1.06	3.60	4.80	3.40	0.82	14.6	1.42
	phenol			0.90	0.30	1.36	1.63	1.75	0.37	2.19	1.63
e	NH_3	0.10	0.29	0.19	1.29	1.79	0.88	1.08	0.41	0.58	0.57
	HCN			5.84	2.19	8.25	6.94	3.36	1.69	64.2	21.0
	HNCO			1.89	0.67	2.61	2.94	1.27	0.70	5.37	1.98
	HONO		0.11	9.40	2.53	9.72	12.7	8.92	1.75	26.9	11.3

289

290

291   When comparing the RFL laboratory scale experiments to the 2018 Ft. Jackson field scale

292   experiments, it is evident that field scale values via the static mode are greater than those of the

293   laboratory, even though the laboratory experiment attempted to replicate Ft. Jackson fuel beds and

294   scenarios. In most cases, a comparison of compounds found in the RFL laboratory burns and the

295   Ft. Jackson 2018 field burns finds Ft. Jackson mixing ratios approximately 4 to 10x greater than

296   those of the RFL 2018 tunnel data. Field scale measurements typically yield more emissions than

297   experiments conducted in the laboratory (Yokelson, 2013; Scharko, 2019b, Weise et al. 2015).

298   However, while the mixing ratios may differ or be larger/smaller, the information describing the

299   composition of the mixture is relative in nature and is contained in log-ratios of the various gases.

300   But analysis of the data as compositional data (Aitchison 1986) is beyond the scope of the present

301   paper. Table 3 displays the minimum and maximum mixing ratio values in ppm for five

302   compounds from the Ft. Jackson studies presented in Scharko et al. (2019a) versus the present

303   RFL laboratory results. Of the five species compared, acetaldehyde, acrolein, and allene all follow

304   the trend of having Ft. Jackson results being significantly higher than the RFL studies by a factor

305   of ~4. Naphthalene, a polycyclic aromatic hydrocarbon (PAH) was the only exception to this trend,

306   having comparable mixing ratio values in the two studies. This anomaly could be attributed to one

307   of naphthalene's pyrolysis formation route as suggested by Fairburn et al., where a single ringed

308   aromatic compound undergoes a Diels-Alder reaction of an alkene (Fairburn et al., 1990; Liu et

309   al., 2017). Of the four compounds compared, naphthalene is the only one to be derived from a

310   secondary reaction, whereas acetaldehyde and acrolein are derived directly from the pyrolysis of

311   cellulose (Stein et al., 1983), while allene is a compound known to be a precursor of aromatic

312   compounds and soot (Frenklach et al., 1983, 1988). As noted, most compounds detected in the

313   RFL laboratory studies yielded ~4 to 10x lower mixing ratios compared to the field scale studies

314   at Ft. Jackson.   Along with naphthalene, however, acetic acid, formaldehyde, isoprene and

315   isobutene were also found to have comparable mixing ratios to those reported in the Ft. Jackson

316   studies.   This could be due to the four compounds being products of secondary reactions, or

317   fragmentation, of species such as lignin, xylan and glucomannan (Collard and Blin, 2014). It

318   should be noted that of the five novel compounds detected in Scharko et al. (2019b), only four

319   were detected in these laboratory scale experiments. Methyl nitrite was not observed (Table 3).

320   This is attributed to the field experiment being on the Ft. Jackson base where there is known to be

321   unexploded ordinance (Scharko et al., 2019b) or possibly due to lower concentration levels that

322   are below the detection limits of the present laboratory-scale experiment.

323   **Table 3.** Calculated minimum and maximum mixing ratios (ppm) for the 10 canister measurements taken at the
324   Ft. Jackson field measurements (Scharko et al., 2019) along with the minimum and maximum mixing ratios
325   (ppm) for the 10 static measurements during the RFL laboratory experiment of acetaldehyde, acrolein, allene,
326   methyl nitrite and naphthalene.

Target Compound	Ft. Jackson calculated mixing ratio (ppm)			RFL calculated mixing ratio (ppm)	
	min	max		min	max
acetaldehyde	34.5	264.8		0.94	73.6
acrolein	14.7	125.7		0.98	26
allene	2.2	37.8		0.12	8.69
methyl nitrite	2.3	21		-	-
naphthalene	1.4	19.9		0.86	14.6

327

328   It is clear that the static method as deployed was not perfect at either isolating strictly the pyrolysis

329   phase gases or capturing extremely high fractions of combustion gases. The method relied heavily

330   on valves being closed prior to the flame front using visual cues as opposed to using other

331   techniques, e.g. thermal IR. While not readily visible to the human eye, radiant and convective

332   heating (as determined by Background-Oriented Schlieren measurements - Aminfar et al 2019)

333   occurred well in advance of the flame front, suggesting this as a possible alternate visualization

334   of pyrolysis gas release (Aminfar 2019). In any case, there is a narrow temporal window for the

335   pre-combustion phase making the valve-close time extremely important. For example, spectra

336   from burns 76 and 78 show largely the detection of only ambient air compounds indicating the

337   valves were closed too early. Conversely, in other samples there is clearly some mixing of both

338   upstream and downstream air before the gas enters the extractive probe. Despite the shortcomings

339   of the static method most of the attempts to obtain pre-combustion gases were successful as

340   evidenced in part by the chemical composition of the isolated gases.

341

342   *3.2 Spectral-Thermal Correlation to Isolate Pyrolysis Phase*

343   Dynamic IR data and visual image acquisition proved advantageous to resolve the different phases

344   of the experiments (e.g. pyrolysis, flaming combustion, smoldering combustion). This was

345   important since MCE is a function of the gas composition and is not unique to phase (i.e., the same

346   value of MCE results if the same relative amounts of CO and CO_2 are observed, whether in the

347   pyrolysis, flaming or smoldering combustion phases) are less appropriate due to the lack of arrival

348   of the flame front and onset of combustion. MCE, defined as $\Delta CO_2/(\Delta CO + \Delta CO_2)$, has many

349   times been used to distinguish phases of combustion, namely flaming vs. smoldering although

350   Ward and Radke (1993) recommended combustion efficiency as the preferred descriptor of the

351   combustion system. MCE has not been used to identify pyrolysis nor should it be for the non-

352   uniqueness described previously. Recent studies have introduced more sophisticated techniques to

353   analyze smoke emissions data with compositional data methods (Weise et al. 2020). However,

354   since primary and secondary pyrolysis occurs both prior to and after the onset of combustion or

355   oxidation, methods such as the MCE are not appropriate. We were not able to use the metric

356   suggested by Sekimoto et al. (2018), namely high temperature vs. low temperature pyrolysis as

357   determined from the acetylene-to-furan ratio due to weak furan signals in the present study due to

358   shortened scan times. The analysis was further exacerbated because furan's strongest vibrational

359   band, the ν_{19} vibrational band near 745 cm^{-1}, corresponding to the C-H out-of-plane bend

360   (Shimanouchi, 1972), was obscured by saturated carbon dioxide lines and thus MALT was not

361   able to generate a satisfactory fit for this microwindow.

362   The pre-flame arrival gases were identified by either of two methods: The first method involved a

363   simple time subtraction of 4.8 s from the recording of the infrared spectrum time stamp and

364   associating that time to the corresponding visual and FLIR thermal infrared video images (Fig. 3).

365   This provided a relatively accurate verification that the gases being investigated were emitted prior

366   to the onset of combustion as seen in Table 4. The second method used the FTIR spectra directly:

367   demarcations for the flame front were denoted by the maximal value obtained for both CO and

368   CO_2 concentrations, i.e. greatest fraction of gas from the combustion phase. From this value the

369   FTIR's scans were selected for pyrolysis corresponding to the ~10 seconds before arrival (~0.1 m

370   distance) of the flame front.

Atmospheric
Measurement
Techniques
Discussions

Open Access

EGU
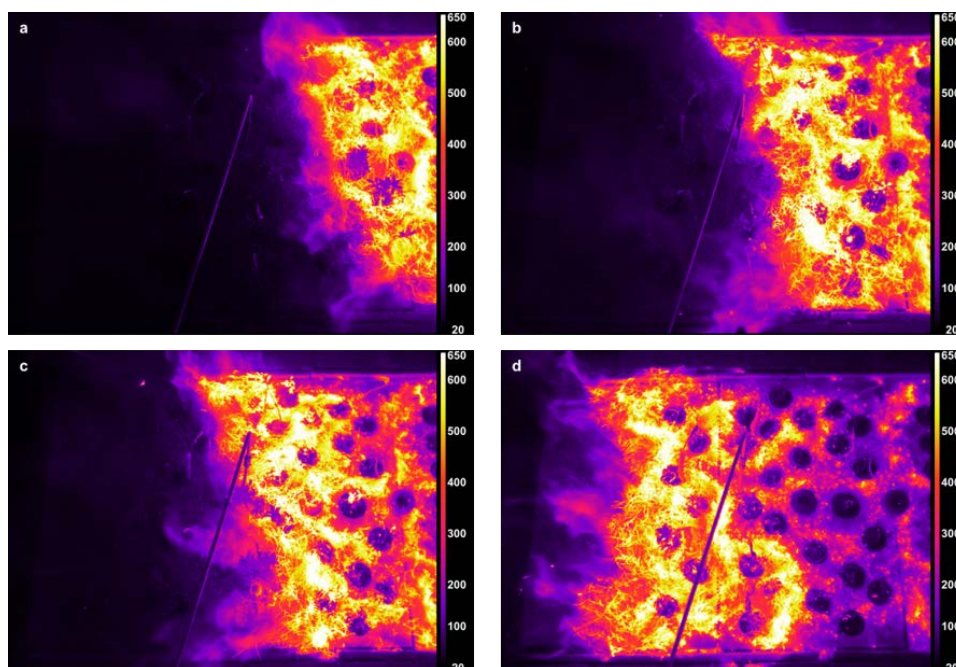
Figure 3. Burn 87 inkberry on longleaf pine needle fuel bed – FLIR thermal imaging for burn progression.
(a) frame corresponding to FTIR scan 5 signaling the pre-combustion phase, (b) frame corresponding to
FTIR scan 16, flame front nearing sample probe, (c) frame corresponding to FTIR scan 21, inkberry bush
consumed by flame, (d) frame corresponding to FTIR scan 44, flame front has passed the probe. Dark
circles are ceramic plant holders.

The FTIR time-resolved scans (including derived chemical mixing ratios) synchronized to the RFL
time-stamped thermal IR temperature images provide insight into the chemical composition of
each burn. As an example, Table 4 pairs data from the two systems for Burn 87. FTIR scan number,
FTIR time stamp, RFL FLIR recorded temperature near the extractive probe, and a selection of
chemical concentrations are shown. The table demonstrates that spectral data for FTIR scans 0-8
saw no significant detections above ambient levels as corroborated by the FLIR images displaying
temperatures range from 40-80 °C (see Table 4 and Figure 3a); the extractive probe is still in the
low temperature region. The gradual increase in mixing ratios for most compounds (excluding
ammonia, which is primarily a smoldering gas) begins after FTIR scan 9. The magenta and orange
colored domains seen in Figure 3b indicate the encroaching flame front and a rise in thermal
temperatures. The frames corresponding to FTIR scans 16-19 display IR temperatures between
175 and 220 °C. In this temperature range compounds associated with the pyrolysis phase such as
acetaldehyde, acetic acid and allene (shown in Table 4) are not only manifest in the IR spectra, but
their mixing ratios rise rapidly. Shortly thereafter the greatest mixing ratios of CO_2 occur at scans

391   20 through 22, indicating the flaming stage; this is corroborated by thermal IR video of the inkberry

392   plant beginning to be fully consumed in flames (Fig 3c). As the flame front progressed down the

393   tunnel, temperatures near the plant holder began to drop with the onset of the smoldering phase as

394   indicated by lower mixing ratios as well as the thermal IR visual seen in Fig. 3d. [We note in

395   Figure 3 that the temperature directly near/above the holders is much cooler due to minimal duff

396   cover and the plants being green.] The video stopped recording at scan 48, when the flame reached

397   the end of the fuel bed although the FTIR continued to collect interferograms to monitor

398   smoldering from the fire.

399

400   **Table 4:** Burn 87 inkberry amongst pine needle fuel bed FTIR scan summary synchronized to FLIR temperature data.
401   Scan number, FTIR time stamp, along with FLIR video emissions temperature at extractive probe accounting for time
402   delay and mixing ratios from carbon dioxide (CO_2), carbon monoxide (CO), ethene (C_2H_4), acetic acid (CH_3COOH),
403   formaldehyde (HCHO), acetaldehyde (CH_3CHO), and phenol (C_6H_6O).

	FTIR Scan Number	FTIR time stamp	4.8 s Delayed FLIR Video Time Stamp	FLIR temperature at inlet (°C)	CO_2 (ppm)	CO (ppm)	C_2H_4 (ppm)	CH_3COOH (ppm)	HCHO (ppm)	CH_3CHO (ppm)	C_6H_6O (ppm)
Ambient	scan 0	10:41:23.69	10:41:18.89	41.4	1548	49.5	2.4	0.0	0.6	-	-
	scan 1	10:41:25.20	10:41:20.40	44.2	1912	74.5	1.9	1.7	0.9	-	-
	scan 2	10:41:26.70	10:41:21.90	51.0	1562	63.7	2.3	1.1	0.3	-	-
	scan 3	10:41:28.21	10:41:23.41	54.9	1290	58.4	1.1	0.5	0.5	-	-
	scan 4	10:41:29.71	10:41:24.91	53.4	1882	63.1	1.2	1.2	0.8	-	-
	scan 5	10:41:31.21	10:41:26.41	63.2	1946	57.0	1.5	1.1	0.4	-	-
	scan 6	10:41:32.72	10:41:27.92	72.8	3811	102	4.7	1.8	1.2	-	-
	scan 7	10:41:34.22	10:41:29.42	77.6	4722	138	2.7	1.9	1.5	-	-
	scan 8	10:41:35.73	10:41:30.93	86.2	3553	109	0.9	2.2	1.4	-	-
Volatilization + Pyrolysis	scan 9	10:41:37.23	10:41:32.43	116.9	2957	97	1.0	2.4	0.7	-	-
	scan 10	10:41:38.73	10:41:33.93	132.1	3360	138	1.8	2.8	1.2	1.4	-
	scan 11	10:41:40.24	10:41:35.44	115.7	7476	246	4.2	2.6	3.6	0.0	-
	scan 12	10:41:41.74	10:41:36.94	121.3	10274	291	6.2	9.0	4.8	4.2	0.7
	scan 13	10:41:43.25	10:41:38.45	183.3	10890	391	11.4	11.5	7.1	1.1	1.6
	scan 14	10:41:44.75	10:41:39.95	159.4	11833	635	23.5	14.5	13.5	3.3	1.5
	scan 15	10:41:46.25	10:41:41.45	163.8	16080	1214	48.5	16.8	28.7	7.2	1.5
	scan 16	10:41:47.76	10:41:42.96	176.9	25757	2217	95.3	16.3	54.4	17.6	1.0
	scan 17	10:41:49.26	10:41:44.46	181.3	31856	2915	129	14.4	70.5	24.0	1.4
	scan 18	10:41:50.77	10:41:45.97	220.1	41291	2878	260	13.1	92.6	34.5	1.4
	scan 19	10:41:52.27	10:41:47.47	219.0	61166	8228	435	12.3	121	44.3	2.1
Flaming Combustion	scan 20	10:41:53.77	10:41:48.97	296.1	79332	11354	747	13.1	178	80.7	2.9
	scan 21	10:41:55.28	10:41:50.48	261.7	54381	9729	1167	17.6	255	140	4.7
	scan 22	10:41:56.78	10:41:51.98	456.1	64077	12954	1025	15.3	185	103	6.0
	scan 23	10:41:58.29	10:41:53.49	429.9	41495	8620	530	15.4	123	63.3	6.3
	scan 24	10:41:59.79	10:41:54.99	516.5	25879	3453	257	15.5	74.5	33.9	6.8
	scan 25	10:42:01.29	10:41:56.49	514.5	15965	3110	116	15.1	45.7	19.6	6.8
	scan 26	10:42:02.80	10:41:58.00	460.1	11819	2416	53.2	15.6	35.2	12.0	5.6
	scan 27	10:42:04.30	10:41:59.50	453.7	8566	1875	36.6	14.7	27.4	6.9	5.2
	scan 28	10:42:05.81	10:42:01.01	448.0	5795	1320	14.5	13.2	21.8	3.0	5.6
	scan 29	10:42:07.31	10:42:02.51	440.2	5235	1302	11.0	14.6	20.0	5.1	4.5
	scan 30	10:42:08.81	10:42:04.01	484.7	3626	916	5.8	15.1	15.0	5.2	4.2
	scan 31	10:42:10.32	10:42:05.52	470.4	2368	570	3.3	11.5	11.1	2.7	3.8
	scan 32	10:42:11.82	10:42:07.02	497.5	1636	377	1.6	10.8	9.4	0.3	3.7
	scan 33	10:42:13.33	10:42:08.53	477.4	1684	399	1.0	9.2	8.8	2.1	3.4
	scan 34	10:42:14.83	10:42:10.03	450.1	1986	519	0.9	10.4	9.5	-1.5	3.0
Smoldering Combustion	scan 35	10:42:16.33	10:42:11.53	397.9	1968	518	0.7	9.9	9.3	2.8	3.2
	scan 36	10:42:17.84	10:42:13.04	410.2	1901	495	1.4	9.6	8.8	0.9	2.8
	scan 37	10:42:19.34	10:42:14.54	401.6	1936	516	1.5	9.2	9.4	0.0	2.7
	scan 38	10:42:20.85	10:42:16.05	358.3	1935	513	1.6	9.0	9.5	1.1	2.8
	scan 39	10:42:22.35	10:42:17.55	341.8	1753	439	1.8	9.7	8.9	1.1	2.3
	scan 40	10:42:23.85	10:42:19.05	320.6	1438	345	1.4	10.4	8.3	-0.5	2.9
	scan 41	10:42:25.36	10:42:20.56	305.9	1224	277	-0.1	10.9	7.4	1.4	2.8
	scan 42	10:42:26.86	10:42:22.06	295.0	1377	324	1.4	11.6	8.2	-2.0	2.4
	scan 43	10:42:28.37	10:42:23.57	272.5	1629	411	1.1	11.8	8.4	0.3	2.4
	scan 44	10:42:29.87	10:42:25.07	258.3	1366	325	0.8	12.8	7.8	2.5	2.7
	scan 45	10:42:31.37	10:42:26.57	260.1	1059	212	0.4	11.9	6.7	3.4	2.7
	scan 46	10:42:32.88	10:42:28.08	238.5	1037	212	0.8	13.1	7.1	0.5	2.3
	scan 47	10:42:34.38	10:42:29.58	223.9	1094	236	0.9	14.4	6.7	1.1	1.2
	scan 48	10:42:35.89	10:42:31.09	226.7	1117	248	1.2	13.1	7.0	-0.4	2.7

404

405

406   As stated, a second method was also used to analyze/corroborate the different stages of the burn,

407   whereby mixing ratios of CO_2, CO and C_2H_4 were analyzed to find their burn maxima (Viatte et

408   al., 2015). The CO_2 elevated mixing ratios (esp. relative to CO) are associated with the hottest,

Atmospheric
Measurement
Techniques
Discussions
Open Access
EGU

409   flaming stage of biomass burns (Yokelson et al., 1996). To temporally isolate the flaming stage,

410   the MCE criteria was employed and values of 88-95% indicative of smoldering were found for the

411   region. Having identified the flaming stage, the pyrolysis stage was estimated by subtracting 6-8

412   seconds from that spectrum with maximal CO/CO_2 emissions, corresponding to ~4 FTIR scans (at

413   1 cm^{-1} resolution).   The agreement between the two methods was quite good and helped to

414   demarcate the stages as seen in Table 4.

415

416   Figure 4 displays the infrared spectral progression of Burn 87, longleaf pine needles with inkberry,

417   bed at 1.0 cm^{-1} resolution looking at two different spectral regions. The CO (and CO_2) profiles are

418   seen in Fig. 4a. Noted on the z-axis is scan 22; scans 20-22 are the time frames where maximal

419   CO_2 and CO emissions were observed; the region is also denoted by red spectral traces. Once the

420   flaming stage had been identified, the pyrolysis phase was then demarcated; in the pyrolysis phase

421   CO was evident (partially from upwind mixing) and was beginning to significantly increase; the

422   stage is indicated by orange traces (scans 16-19) in Figure 4. Other stages assigned were noted as

423   the pre-flame stage where ΔCO and ΔCO_2 were near zero in the FTIR data and are seen as scans

424   0-8 with purple traces. Blue traces correspond to the smoldering phase of combustion, where CO_2

425   mixing ratios decreased, the flame front had passed the extractive probe and MCE values were on

426   the order of 85-75%. The spectral profile and mixing ratios of ethene (C_2H_4) were also used to

427   evaluate the time-resolved FTIR data. (Johnson et al. 1993) This lightweight hydrocarbon is a

428   product of primary pyrolysis and if detected can be used to determine certain stages of the burn

429   (e.g. Yang et al., 2007). Figure 4b displays primarily the ν_7 band of ethene at 949.4 cm^{-1}

430   (Shimanouchi, 1972). Ethene reached its maxima mixing ratio at scan 22 (red traces) before it

431   quickly disappeared, being a pyrolysis gas that was oxidized by the flame. It was first seen to

432   appear as early as scan 13 (green traces) but became clearly evident in scan 16 (orange traces,

433   pyrolysis phase) and continued to grow. The rapid disappearance of C_2H_4 upon combustion is

434   similar to that of formaldehyde and acetaldehyde (Table 4) whose concentrations also dropped

435   after scan 23, but the disappearance is juxtaposed with acetic acid whose values remained

436   ~constant throughout the flaming and smoldering phases. As seen in the IR data, the C_2H_4 gas

437   signal corroborated that ethene is a key product of the primary pyrolysis phase. Other compounds

438   showing significant signals in this time domain and described as pyrolysis gases include acrolein

439   and allene. (Scharko 2019a; Akagi et al., 2013; Frenklach et al. 1983, 1988; Stein et al., 1983;

440   Koss et al., 2018; Brilli et al., 2014).
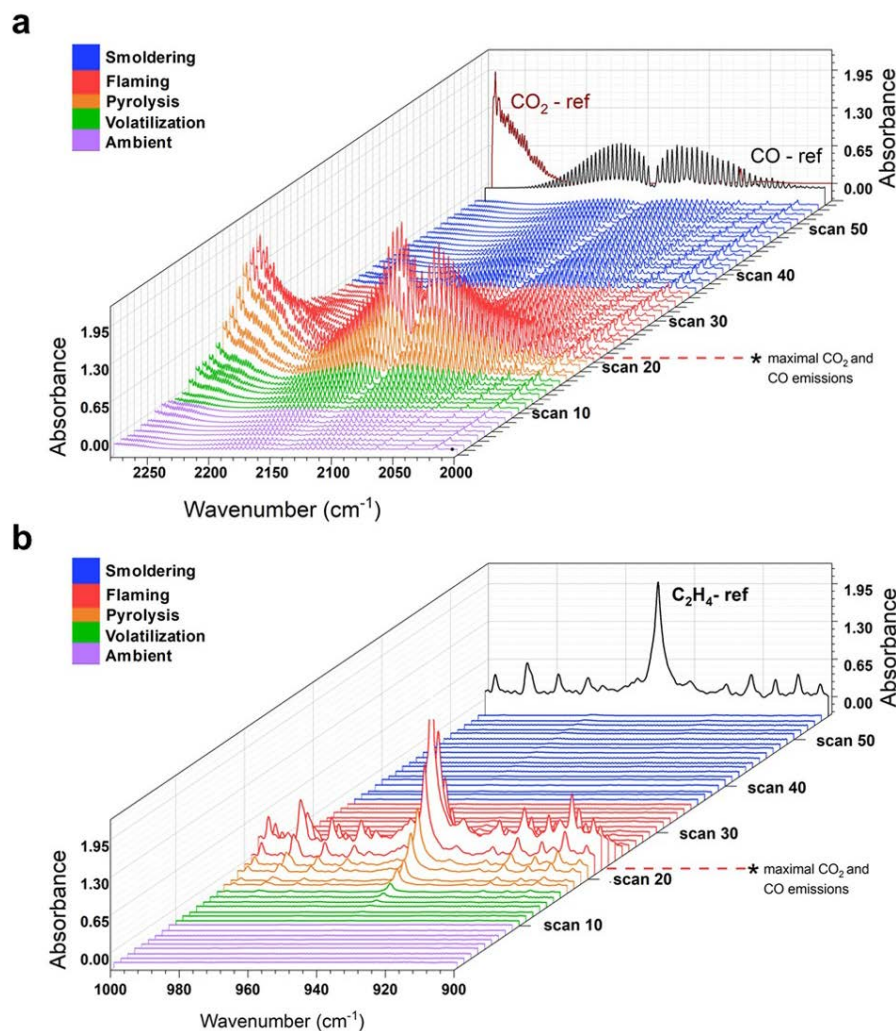
Figure 4. Burn 87, inkberry with longleaf pine needles: a) CO and CO_2 spectral profile from 2250-2000 cm⁻¹. Purple traces indicate the ambient stage, green and orange traces indicate the pre-combustion/pyrolysis stage, red spectral traces indicate the flaming stage and blue traces indicate smoldering. b) Largely C_2H_4 spectral waterfall plot from 1000-900 cm⁻¹ with accompanying C_2H_4 reference spectrum as black trace.

447   The two methods to determine the pyrolysis, flaming, combustion and smoldering phases yielded

448   congruous results: The isolated burn stages determined from method one, in which FTIR gas-

449   phase data were synchronized to the FLIR thermal imaging, and from method two, using the FTIR

450   time-resolved data only, were found to be virtually identical. This is evidenced by linking the scans

Atmospheric
Measurement
Techniques
Discussions

Open Access
EGU

451   determined to be in the pyrolysis phase (scans 16-19) using method two as seen in Fig. 4, with the

452   temperature data recorded by the FLIR using method one and seen in Table 4. For these scans,

453   the temperature profile ranges from 175-220 °C, corresponding to temperatures associated with

454   first stages of pyrolysis.

455   For most analytes biomass burning gas mixing ratios, the concentration values observed at the

456   peak of the dynamic measurements values were significantly greater than for the concentrations

457   recorded in the static measurements. The dynamic experiments were of course carried out for the

458   duration of the burn, whereas the static burns (in an effort to characterize pre-combustion phases)

459   attempted to isolate a specific time when the pyrolyzate concentrations were maximized.

460   Analyzing the data using the dynamic technique allowed for confirmation of certain compounds

461   such as naphthalene, allene, acetaldehyde, and acrolein as compounds that appeared during the

462   pyrolysis phase. These compounds, which have been previously detected as pyrolysis gases using

463   FTIR for field plot burns, (Scharko et al. 2019) were again observed during these laboratory scale

464   tests and in almost all cases appeared before the flame front encroached on the sampling probe.

3.3 Dynamic Detection of Phenol in the Pre-combustion Through Smoldering Stages

466   In the present study phenol (C_6H_6O) was detected during several burns; its origin ascribed to the

467   pyrolysis of lignin(s) (Kibet et al. 2012, Hawthorne et al. 1989) and has been mostly observed

468   using other techniques such as gas chromatography mass spectrometry (GC-MS). (Saiz-Jimenez

469   et al. 1986) Phenol and phenolic compounds are also known to contribute to the formation of

470   secondary organic aerosols. (Yee et al., 2013) It has been observed in simple pyrolysis

471   experiments, emanating from both pine and spruce species (e.g. Saiz-Jimenez and De Leeuw,

472   1986, Ingemarsson et al., 1998). In addition to simply pyrolytic emissions, phenol has also been

473   identified as a common component of tar as a pyrolysis product. In biomass burning, phenol has

474   been observed using both FTIR and other methods, (Gilman et al. 2015, Yokelson et al. 2013), e.g.

475   proton-transfer mass spectrometry (PTR-MS) and GC-MS. In 2013 phenol was detected in a

476   closed cell, airborne FTIR field experiment but not in an open-path FTIR lab experiment

477   (Yokelson et al. 2013). The absence of C_6H_6O in the lab experiment was attributed to the lack of

478   consumption of rotten wood as fuel. In those studies, airborne phenol emissions measured in the

479   field with closed-cell FTIR were also noted as being 2 to 4x greater than the phenol emissions

480   captured by PTR-MS in the laboratory.

481   In the present experiments, phenol was detected in 8 of the 10 static measurements (recall that two

482   of the static measurements only showed ambient gases due to early closure of the valves). Figure

483   5 demonstrates the static spectrum from Burn 89, corresponding to the burning of longleaf pine

484   with inkberry. Seen in Fig. 5 are the experimental spectrum (blue trace) and also the reference

485   spectrum of acetic acid (green trace). After subtraction of the CH_3COOH vapor spectrum, the

486   residual contained two small peaks which were readily identified as phenol vapor via the ν_{15}

487   vibrational band near 1176.2 cm^{-1}, as well as the ν_{16} band at 1150.2 cm^{-1} (Keresztury et al., 1998).

488   The phenol reference spectrum from the PNNL spectral library (red trace) was then subtracted

489   from that residual (purple trace) with an overall residual that is mostly noise (black trace). [For the

490   dynamic spectra the process is repeated for each of the individual spectral time slices, represented

491   by scan number using the concentration of phenol determined by the MALT program.] To confirm

492   the spectral analysis, in each case the mixing ratio calculated by MALT was converted to a

493   spectrum by multiplying by the appropriate concentration path length factor; the predicted

494   spectrum was visually compared to the actual data.
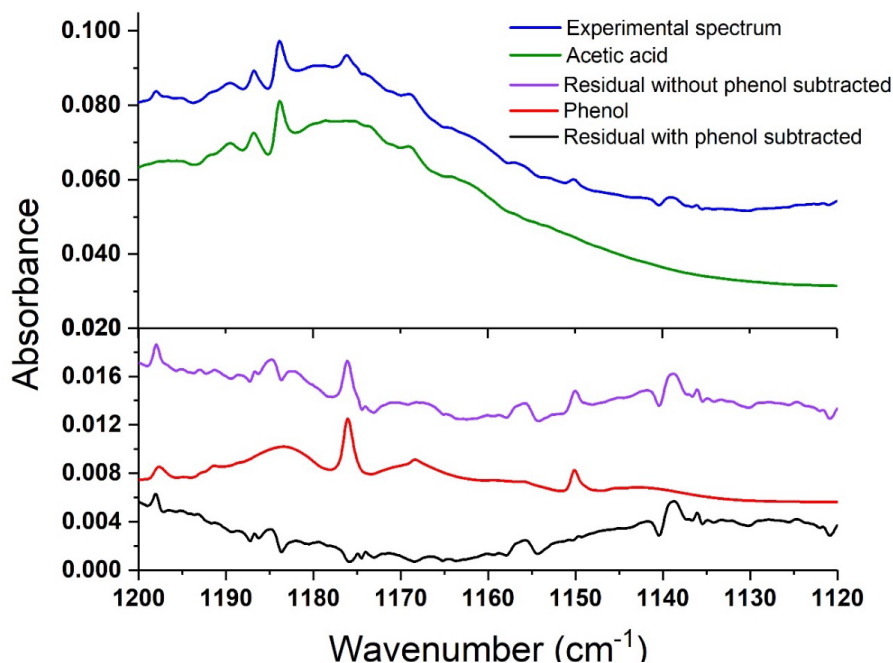
495

496   **Figure 5.** Static spectrum obtained from Burn 89 (1 kg longleaf pine needles with inkberry). The blue trace
497   is the FTIR experimental spectrum, the green trace the reference spectrum of acetic acid, the purple trace
498   the residual after acetic acid subtraction, the red trace the reference spectrum of phenol and the black trace
499   residual after phenol optimization/subtraction.

500 Phenol was also detected using the dynamic method and Figure 6 displays a series of dynamic

501 spectra recorded for Burn 87. The spectra in the left frame (a) are individual spectra after the acetic

502 acid (CH_3COOH) spectral component has been subtracted from the spectrum for each time slice,

503 all recorded at 1.0 cm^{-1} resolution with 54 total measurements recorded at Δt=1.5 seconds. While

504 the spectral noise is still significant, the presence of phenol peaks, particularly the ν_{16} Q-branch at

505 1176.5 cm^{-1} and the ν_{15} peak at 1150.2 cm^{-1}, are evident. Optimization for the phenol mixing ratio

506 in each spectrum allowed for its calculation in individual time slices and the derived phenol-only

507 spectra are presented as a waterfall plot in the right frame (b). The first clear evidence of phenol is

508 seen in scans 14 to 18, before reaching a maximum concentration of 6.9 ppm in scan 24; this is

509 observed in the right frame of Figure 6, coinciding approximately with maximal CO_2 concentration

510 (scan 22), indicating the greatest ratio of smoke/ambient air in the gas cell.
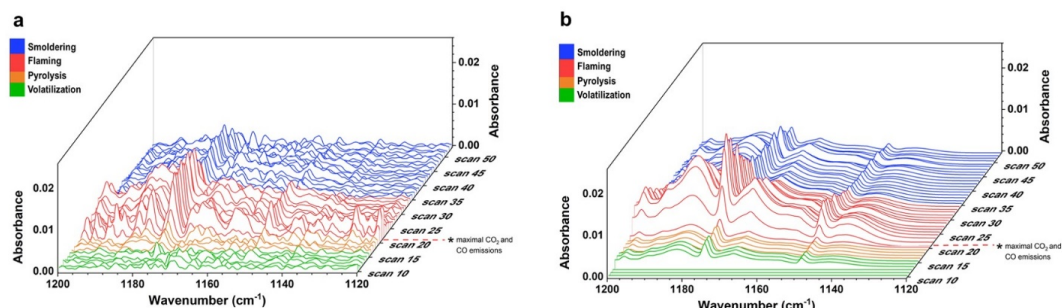
511

512 **Figure 6.** Burn 87 –longleaf pine needles with inkberry fuel bed during dynamic mode. Measured and
513 scaled burn spectra showing the progression of phenol during the time resolved study. Acetic acid and
514 water spectral features have been removed in Frame a) with the phenol-only derived mixing ratio spectra
515 in Frame b.

516 Figure 6 displays the rapid increase of phenol vapor due to the approaching flame front from scan

517 14 (t = 22.5 s) to its maximal mixing ratio in scan 24 (t = 36 s) followed by a longer gradual phenol

518 decay with time. This can be juxtaposed with the ethene mixing ratios (seen in Figure 4) that fall

519 to nearly zero with the onset of combustion; the ethene is consumed by the flame propagation.

520 Prior to scan 14 in Figure 6b, minimal phenol is observed relative to the noise level and are thus

521 fit as zero concentration. Phenol contributions for scans 16-19 can be associated with the pyrolysis

522 phase of the burn and not combustion. Phenol is one of the major products of 1,2-benzenediol

523 pyrolysis with maximum yield reported at 800 °C (Ledesma et al. 2002; Thomas et al. 2007). It is

524 important to note that both temperature and rate of heating influence the composition and yield of

525 pyrolysis products. Evidenced in Figure 6, the thermal imaging associated with FTIR scan 17

Atmospheric
Measurement
Techniques
Discussions

526 shows a temperature of ~200 °C which is indicated in Kibet et al. (2012) to be within the

527 temperature range of pyrolysis of lignin: 200 to 400 °C. Shortly thereafter, phenol mixing ratios

528 rapidly increase and reach a maximal mixing ratio of 6.9 ppm at scan 24. At scan 24 the flame

529 front has already reached the extractive probe and thus the maximum intake of smoke and ambient

530 air is achieved; temperature of the fuel bed is ca. 600 °C, consistent with the flaming phase. The

531 gradual decay in phenol production as the flame front passes could be due to several factors: (i) an

532 increased temperature required for complete combustion of the C_6H_6O (ii) residence time of

533 phenol, (iii) phenol production in the smoldering phase as a tar/char, (iv) adsorption to walls of the

534 stainless steel tubing and cell. A cross-section of Figure 6 shows the rapid onset of phenol

535 production at the temperatures followed by a gradual decay in concentration: this is indicative of

536 phenol production throughout the burning of inkberry as a species.

537
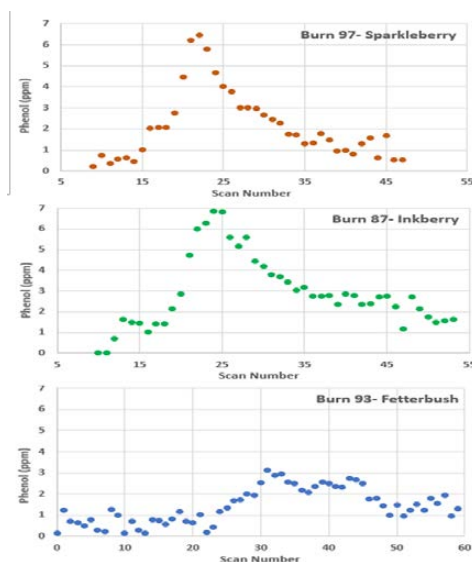
Figure 7. Temporal mixing ratios of phenol for different shrub species. Phenol mixing ratios plotted over time indicated by scan number for Burn 97 sparkleberry (red), Burn 87 inkberry (green), and Burn 20 fetterbush (blue) all on longleaf pine straw bed.

541 The shape of the temporal profile yields information as to the production of phenol throughout the

542 evolution of burning. Figure 7 shows the progression of phenol concentration following its first

543 observed presence in the burn. These graphs are effectively a cross-section of Figure 6, showing

544 the progression of the height of the phenol peak (directly correlated to phenol concentration)

545 throughout the burn (with time being represented by scan number in both cases). The level of

546   phenol generation was observed to vary between plant species. Temporal profiles of phenol

547   concentration were constructed for burns with three different species: sparkleberry, inkberry, and

548   fetterbush. These plots illustrate a range of behavior with inkberry and sparkleberry having similar

549   temporal profiles and similar maxima of ca. 6.5 ppm and fetterbush having a different temporal

550   profile. It is important to note that Burn 97 was measured at 0.6 cm^{-1}, while burns 87 and 93 were

551   measured at 1.0 cm^{-1}, although the profile of burn 97 is consistent with that of burn 87. [We do not

552   believe the small change in resolution affects the recovered mixing ratios.] Demonstrated in Figure

553   7, trace amounts of phenol appear at the onset of combustion and throughout the pyrolysis phase.

554   Phenol reaches its highest concentrations, however, during the flaming stage as all three temporal

555   profiles reach maximum during the latter stages of the burn. Moreover, phenol remains throughout

556   the duration of the burn and is not consumed by secondary reactions, as is e.g. ethene. For these

557   three burns, fetterbush was observed to have the lowest maximum concentration of phenol, 3.1

558   ppm, of the three species, while sparkleberry and inkberry had similar maxima (as well as similar

559   temporal profiles).

560   The observed differences of phenol in both temporal profile and overall peak concentrations could

561   arise due to differences in leaf structure and shape, or possibly due to differences in leaf/plant

562   composition. Pyrolytic production of phenol has been previously attributed to multiple

563   components of plant composition, including phenol content, lignin content and the amount of

564   cellulose in each plant species. Therefore, varying phenols, lignin, and cellulose in these plant

565   species could be the source of phenol concentration variability for each burn. The physical

566   composition of multiple plant species, including inkberry and fetterbush was analyzed by Matt and

567   Dietenberger (2020); it was shown that inkberry has 2.6 times the percentage of phenol by

568   composition (9.0%) than fetterbush (3.4%) Although sparkleberry was not included in that study,

569   it can be suggested that the compositions of inkberry and sparkleberry are similar due to observed

570   phenol in this experiment as well as plant characteristics. Sparkleberry, a member of the *Vaccinium*

571   genus, contains many species collectively known as blueberries which are known to contain high

572   levels of phenolic compounds in the fruits (e.g. Prior et al 1998). This study and the results of Matt

573   and Dietenberger support the present hypothesis that peak concentrations of phenol are highest for

574   sparkleberry and inkberry due to higher phenolic content in the plants.

575   **4. Summary**

576 The analytical methods used in this study attempt to provide a detailed view of prescribed burning
577 by enlisting two different FTIR acquisition modes, static and dynamic. By capturing a "snapshot"
578 of a single burn experiment, used in the static method, one can discern the gases with higher
579 specificity and in turn decipher complex spectra by use of chemometrics to extract compounds
580 with high concentrations leaving behind a residual to be analyzed. Lower resolution may hinder
581 these efforts and allow compounds that are present at lower mixing ratios to be obscured by higher
582 absorbing compounds, e.g., carbon dioxide, water, and ethene. In this study we were able to detect
583 additional compounds e.g. phenol, benzene, and allene with greater confidence. However, in
584 gaining specificity there is a loss of time resolution and this is where the dynamic method becomes
585 advantageous. The FTIR dynamic acquisition method when synchronized to thermal imaging,
586 while lower in sensitivity, allows for an overall profile of the burn and can help assign phases to
587 the dynamic stages of the flame. That is, the dynamic method in conjunction with thermal IR
588 imaging provides a more detailed description as temperature and chemical composition profiles
589 can be correlated and assigned to certain phases of the burns. In this study pyrolysis, flaming and
590 smoldering combustion were identified using these new techniques which can aide in the
591 improvement of fire behavior models used by land managers to conduct prescribed fires.

592 *Data availability.* Data are not publicly available as data release has not been authorized by sponsor
593 of this research.

594 *Competing interests.* No competing interests.

599

REFERENCES

Agee, J. K.: Fire and pine ecosystems, in Ecology and Biogeography of Pinus, edited by D. M. Richardson, pp. 193–218, Cambridge University Press, Cambridge, U.K., 2000.

Aitchison, J.: The statistical analysis of compositional data, Chapman and Hall, London ; New York., 1986.

Akagi, S. K., Yokelson, R. J., Burling, I. R., Meinardi, S., Simpson, I., Blake, D. R., McMeeking, G. R., Sullivan, A., Lee, T., Kreidenweis, S., Urbanski, S., Reardon, J., Griffith, D. W. T., Johnson, T. J., and Weise, D. R.: Measurements of reactive trace gases and variable O3 formation rates in some South Carolina biomass burning plumes, Atmos. Chem. Phys., 13, 1141-1165, 2013.

Akagi, S. K., Burling, I. R., Mendoza, A., Johnson, T. J., Cameron, M., Griffith, D. W. T., Paton-Walsh, C., Weise, D. R., Reardon, J., and Yokelson, R. J.: Field measurements of trace gases emitted by prescribed fires in southeastern US pine forests using an open-path FTIR system, Atmos. Chem. Phys., 14, 199-215, 2014.

Alves, C. A., Gonçalves, C., Pio, C. A., Mirante, F., Caseiro, A., Tarelho, L., Freitas, M. C., and Viegas, D. X.: Smoke emissions from biomass burning in a Mediterranean shrubland, Atmos. Environ., 44, 3024-3033, 2010.

Aminfar, A., Cobian-Iñiguez, J., Ghasemian, M., Espitia, N. R., Weise, D. R. and Princevac, M.: Using Background-Oriented Schlieren to Visualize Convection in a Propagating Wildland Fire, Combustion Science and Technology, 1–21, doi:10.1080/00102202.2019.1635122, 2019.

Aminfar, A.: Application of Computer Vision to Transport Phenomena, Ph.D., University of California, Riverside., 2019.

Amini, E., Safdari, M.-S., DeYoung, J. T., Weise, D. R. and Fletcher, T. H.: Characterization of pyrolysis products from slow pyrolysis of live and dead vegetation native to the southern United States, Fuel, 235, 1475–1491, doi:10.1016/j.fuel.2018.08.112, 2019.

Barbour, M. G. and Billings, W. D., Eds.: North American terrestrial vegetation, 2. ed., Cambridge Univ. Press, Cambridge., 2000.

Behm, A., Duryea, M. L., Long, A. J. and Zipperer, W. C.: Flammability of native understory species in pine flatwood and hardwood hammock ecosystems and implications for the wildland–urban interface, International Journal of Wildland Fire, 13(3), 355–365, doi:10.1071/WF03075, 2004.

Bist, H. D., Brand, J. C. D. and Williams, D. R.: The Vibrational Spectrum and Torsion of Phenol, J. Mole. Spec, 24, 402-412, 1967.

Biswell, H. H.: Prescribed burning in California wildlands vegetation management, Berkeley, CA: University of California Press; p. 255, 1989.

635 Brilli, F., Gioli, B., Ciccioli, P., Zona, D., Loreto, F., Janssens, I. A., and Ceulemans, R.: Proton
636 Transfer Reaction Time-of-Flight Mass Spectrometric (PTR-TOF-MS) determination of volatile
637 organic compounds (VOCs) emitted from a biomass fire developed under stable nocturnal
638 conditions, Atmos. Environ., 97, 54-67, 2014.

639 Burgan, R. E. and Susott, R. A.: Influence of sample processing techniques and seasonal
640 variation on quantities of volatile compounds of gallberry, saw-palmetto and wax myrtle,
641 International Journal of Wildland Fire, 1(1), 57–62, doi:10.1071/WF9910057, 1991.

642 Burling, I. R., Yokelson, R. J., Griffith, D. W. T., Johnson, T. J., Veres, P., Roberts, J. M.,
643 Warneke, C., Urbanski, S. P., Reardon, J., Weise, D. R., Hao, W. M. and de Gouw, J.:
644 Laboratory measurements of trace gas emissions from biomass burning of fuel types from the
645 southeastern and southwestern United States, Atmos. Chem. Phys., 10(22), 11115–11130,
646 doi:10.5194/acp-10-11115-2010, 2010.

647 Burling, I. R., Yokelson, R. J., Akagi, S. K., Urbanski, S. P., Wold, C. E., Griffith, D. W. T.,
648 Johnson, T. J., Reardon, J., and Weise, D. R.: Airborne and ground-based measurements of the
649 trace gases and particles emitted by prescribed fires in the United States, Atmos. Chem. Phys.,
650 11, 12197-12216, 2011.

651 Bytnerowicz, A., Arbaugh, M. A., Andersen, C. K. and Riebau, A. R., Eds.: Wildland fires and
652 air pollution, Elsevier, Amsterdam ; Boston., 2009.

653 Carter, M. C. and Foster, C. D.: Prescribed burning and productivity in southern pine forests: a
654 review, Forest Ecol. Manage., 191, 93–109, 2004.

655 Christensen, N. L.: Vegetation of the Southeastern Coastal Plain, in North American Terrestrial
656 Vegetation, edited by M. G. Barbour and W. D. Billings, pp. 397–448, Cambridge University
657 Press, New York, NY., 2000.

658 Christian, T. J., Kleiss, B., Yokelson, R. J., Holzinger, R., Crutzen, P. J., Hao, W. M., Shirai, T.,
659 and Blake, D. R.: Comprehensive laboratory measurements of biomass-burning emissions: 2.
660 First intercomparison of open-path FTIR, PTR-MS, and GC-MS/FID/ECD, J. Geophys. Res.
661 Atmos., 109, 2004.

662 Chi, C. T., Horn, D. A., Zanders, D. L., Opferkuch, R. E., Nyers, J. M., Pierovich, J. M., Lavdas,
663 L. G., McMahon, C. K., Nelson, R. M., Jr., Johansen, R. W. and Ryan, P. W.: Source
664 Assessment: Prescribed Burning, State of the Art, Environmental Protection Technology, United
665 States Environmental Protection Agency, Research Triangle Park, NC. [online] Available from:
666 nepis.epa.gov, 1979.

667 Cohen, S., Hall, J. and Hiers, J. K.: Fire Science Strategy, Strategic Environmental Research and
668 Development Program, Resource Conservation and Climate Change Program Area, Washington,
669 D.C. [online] Available from: https://serdp-
670 estcp.org/content/download/30210/291748/file/Fire%20Science%20Strategy.pdf, 2014.

Collard, F.X. and Blin, J.: A review on pyrolysis of biomass constituents: Mechanisms and composition of the products obtained from the conversion of cellulose, hemicelluloses and lignin. Renewable and Sustainable Energy Reviews, 38, pp.594-608, 2014.

Crutzen, P. J. and Goldammer, J. G., Eds.: Fire in the environment: the ecological, atmospheric, and climatic importance of vegetation fires: report of the Dahlem Workshop, held in Berlin, 15-20 March 1992, Wiley, Chichester, England ; New York., 1993.

Depew, C. A., Mann, M. J. and Corlett, R. C.: A Laboratory Simulation of Wood Pyrolysis Under Field Conditions, Combustion Science and Technology, 6(4), 241–246, doi:10.1080/00102207208952326, 1972.

Di Blasi, C.: Modeling chemical and physical processes of wood and biomass pyrolysis, Progress in Energy and Combustion Science, 34(1), 47–90, doi:10.1016/j.pecs.2006.12.001, 2008.

Dimitrakopoulos, A. P.: Thermogravimetric analysis of Mediterranean plant species, Journal of Analytical and Applied Pyrolysis, 60(2), 123–130, doi:10.1016/S0165-2370(00)00164-9, 2001.

Fairburn, J. A., Behie, L. A., and Svrcek, W. Y.: Ultrapyrolysis of n-hexadecane in a novel micro-reactor, FUEL, 69, 1537-1545, 1990.

Frenklach, M., Taki, S., Durgaprasad, M. B., and Matula, R. A.: Soot formation in shock-tube pyrolysis of acetylene, allene, and 1, 3-butadiene, Combust. Flame, 54, 81–101, 1983.

Frenklach, M., Yuan, T., and Ramachandra, M. K.: Soot formation in binary hydrocarbon mixtures, Energy Fuels, 2, 462–480, 1988.

Gilman, J. B., Lerner, B. M., Kuster, W. C., Goldan, P. D., Warneke, C., Veres, P. R., Roberts, J. M., de Gouw, J. A., Burling, I. R., and Yokelson, R. J.: Biomass burning emissions and potential air quality impacts of volatile organic compounds and other trace gases from fuels common in the US, Atmos. Chem. Phys., 15, 13915-13938, 2015.

Griffith, D. W. T.: MALT5 User guide Version 5.5.9 2016.

Goode, J. G., Yokelson, R. J., Susott, R. A., and Ward, D. E.: Trace gas emissions from laboratory biomass fires measured by open-path Fourier transform infrared spectroscopy: Fires in grass and surface fuels, J. Geophys. Res. Atmos., 104, 21237-21245, 1999.

Goode, J. G., Yokelson, R. J., Ward, D. E., Susott, R. A., Babbitt, R. E., Davies, M. A., and Hao, W. M.: Measurements of excess O3, CO2, CO, CH4, C2H4, C2H2, HCN, NO, NH3, HCOOH, CH3COOH, HCHO, and CH3OH in 1997 Alaskan biomass burning plumes by airborne Fourier transform infrared spectroscopy (AFTIR), J. Geophys. Res. Atmos., 105, 22147-22166, 2000.

Gordon, I. E., Rothman, L. S., Hill, C., Kochanov, R. V., Tan, Y., Bernath, P. F., Birk, M., Boudon, V., Campargue, A., Chance, K. V., Drouin, B. J., Flaud, J.-M., Gamache, R. R., Hodges, J. T., Jacquemart, D., Perevalov, V. I., Perrin, A., Shine, K. P., Smith , M.-A. H., Tennyson, J., Toon, G. C., Tran, H., Tyuterev, V. G., Barbe, A., Császár, A. G., Devi, V. M.,

716 Furtenbacher, T., Harrison, J. J., Hartmann, J.-M., Jolly, A., Johnson, T. J., Karman, T., Kleiner,
717 I., Kyuberis, A. A., Loos, J., Lyulin, O. M., Massie, S. T., Mikhailenko, S. N., Moazzen-Ahmadi,
718 N., Müller, H. S. P., Naumenko, O. V., Nikitin, A. V., Polyansky, O. L., Rey, M., Rotger, M.,
719 Sharpe, S. W., Sung, K., Starikova, D., S.A. Tashkun, S. A., Van der Auwera, J., Wagner, G.,
720 Wilzewski, J., Wcisło, P., Yu, S., and Zak, E. J.: The HITRAN2016 molecular spectroscopic
721 database, J. Quant. Spectrosc. Radiat. Transfer, 203, 3-69, 2017.
722
723 Guérette, É.-A., Paton-Walsh, C., Desservettaz, M., Smith, T. E. L., Volkova, L., Weston, C. J.
724 and Meyer, C. P.: Emissions of trace gases from Australian temperate forest fires: emission
725 factors and dependence on modified combustion efficiency, Atmos. Chem. Phys., 18, 3717-3735,
726 doi: 10.5194/acp-18-3717-2018, 2018.
727
728 Hardy, C. C., Ottmar, R. D., Peterson, J. L., Core, J. E. and Seamon, P.: Smoke management
729 guide for prescribed and wildland fire; 2001 ed., PMS 420-2 National Wildfire Coordinating
730 group, Boise, ID. 226 pp., 2001.
731
732 Hatch, L. E., Yokelson, R. J., Stockwell, C. E., Veres, P. R., Simpson, I. J., Blake, D. R.,
733 Orlando, J. J., and Barsanti, K. C.: Multi-instrument comparison and compilation of non-
734 methane organic gas emissions from biomass burning and implications for smoke-derived
735 secondary organic aerosol precursors, Atmos. Chem. Phys., 17, 1471-1489, 2017.
736
737 Hawthorne, S. B., Krieger, M. S., Miller, D. J., and Mathiason, M. B.: Collection and
738 quantitation of methoxylated phenol tracers for atmospheric pollution from residential wood
739 stoves, Environ. Sci. Technol., 23, 470-475, https://doi.org/10.1021/es00181a013, 1989.
740
741 Hough, W. A.: Caloric value of some forest fuels of the southern United States, Research Note,
742 USDA Forest Service, Southeastern Forest Experiment Station, Asheville, NC. [online]
743 Available from: http://www.treesearch.fs.fed.us/pubs/2778, 1969.
744
745 Hurst, D. F., Griffith, D. W. T., Carras, J. N., Williams, D. J., and Fraser, P. J.: Measurements of
746 Trace Gases Emitted by Australian Savanna Fires During the 1990 Dry Season, J. Atmos.
747 Chem., 18, 33-56, 1994a.
748
749 Hurst, D. F., Griffith, D. W. T., and Cook, G. D.: Trace gas emissions from biomass burning in
750 tropical Australian savannas, J. Geophys. Res., 99, 16441-16456, 1994b.
751
752 Ingemarsson, A., Nilsson, U., Nilsson, M., Pedersen, J. R., and Olsson, J. O.: Slow Pyrolysis of
753 Spruce and Pine Samples Studied with GC/MS and GC/FTIR/FID, Chemosphere, 36-14, 2879-
754 2889, 1998.
755
756 Johnson, T. J., Simon, A., Weil, J. M. and Harris, G. W., "Applications of time-resolved step-
757 scan and rapid-scan FT-IR spectroscopy: Dynamics from ten seconds to ten nanoseconds"
758 Applied Spectroscopy, 47, 1376, (1993).
759

760   Johnson, T. J., Masiello, T., and Sharpe, S. W.: The quantitative infrared and NIR spectrum of
761   CH2I2 vapor: vibrational assignments and potential for atmospheric monitoring, Atmos. Chem.
762   Phys., 6, 2581-2591, 2006.

763

764   Johnson, T. J., Profeta, L. T. M., Sams, R. L., Griffith, D.W. T., and Yokelson, R. L.: An
765   infrared spectral database for detection of gases emitted by biomass burning, Vib. Spectrosc., 53,
766   97–102, 2010.

767

768   Jolly, W. M., Hintz, J., Linn, R. L., Kropp, R. C., Conrad, E. T., Parsons, R. A. and Winterkamp,
769   J.: Seasonal variations in red pine (*Pinus resinosa*) and jack pine (*Pinus banksiana*) foliar
770   physio-chemistry and their potential influence on stand-scale wildland fire behavior, Forest
771   Ecology and Management, 373, 167–178, doi:10.1016/j.foreco.2016.04.005, 2016.

772

773   Jolly, W. M., Parsons, R. A., Hadlow, A. M., Cohn, G. M., McAllister, S. S., Popp, J. B.,
774   Hubbard, R. M. and Negron, J. F.: Relationships between moisture, chemistry, and ignition of
775   *Pinus contorta* needles during the early stages of mountain pine beetle attack, Forest Ecology
776   and Management, 269, 52–59, doi:10.1016/j.foreco.2011.12.022, 2012.

777

778   Karl, T. G., Christian, T. J., Yokelson, R. J., Artaxo, P., Hao, W. M., and Guenther, A.: The
779   Tropical Forest and Fire Emissions Experiment: method evaluation of volatile organic compound
780   emissions measured by PTR-MS, FTIR, and GC from tropical biomass burning, Atmos. Chem.
781   Phys., 7, 5883-5897, 2007.

782

783   Keresztury, G., Billes, F., Kubinyi, M. and Sundius, T.: A Density Functional, Infrared Linear
784   Dichroism, and Normal Coordinate Study of Phenol and its Deuterated Derivatives: Revised
785   Interpretation of the Vibrational Spectra, J. Phys. Chem, 102, 1371-1380, 1998.

786

787   Kibet, J., Khachatryan, L., and Dellinger, B.: Molecular products and radicals from pyrolysis of
788   lignin, Environ. Sci. Technol., 46, 12994-13001, 2012.

789

790   Kochanov, R.V., Gordon, I.E., Rothman, L.S., Shine, K.P., Sharpe, S.W., Johnson, T.J.,
791   Wallington, T.J., Harrison, J.J., Bernath, P.F., Birk, M. and Wagner, G.: Infrared absorption
792   cross-sections in HITRAN2016 and beyond: Expansion for climate, environment, and
793   atmospheric applications. Journal of Quantitative Spectroscopy and Radiative Transfer, 230,
794   pp.172-221. 2019.

795

796   Koss, A. R., Sekimoto, K., Gilman, J. B., Selimovic, V., Coggon, M. M., Zarzana, K. J., Yuan,
797   B., Lerner, B. M., Brown, S. S., Jimenez, J. L., Krechmer, J., Roberts, J. M., Warneke, C.,
798   Yokelson, R. J., and de Gouw, J.: Non-methane organic gas emissions from biomass burning:
799   identification, quantification, and emission factors from PTR-ToF during the FIREX 2016
800   laboratory experiment, Atmos. Chem. Phys., 18, 3299, 2018.

801

802   Ledesma, E. B., Marsh, N. D., Sandrowitz, A. K. and Wornat, M. J.: An experimental study on
803   the thermal decomposition of catechol, Proceedings of the Combustion Institute, 29(2), 2299–
804   2306, doi:10.1016/S1540-7489(02)80280-2, 2002.

805

806   Liu, X., Huey, L. G., Yokelson, R. J., Selimovic, V., Simpson, I. J., Müller, M., Jimenez, J. L.,
807   Campuzano-Jost, P., Beyersdorf, A. J., Blake, D. R., Butterfield, Z., Choi, Y., Crounse, J. D.,
808   Day, D. A., Diskin, G. S., Dubey, M. K., Fortner, E., Hanisco, T. F., Hu, W., King, L. E.,
809   Kleinman, L., Meinardi, S., Milkoviny, T., Onasch, T. B., Palm, B. B., Peischl, J., Pollack, I. B.,
810   Ryerson, T. B., Sachse, G. W., Sedlacek, A. J., Shilling, J. E., Springston, S., St. Clair, J. M.,
811   Tanner, D. J., Teng, A. P., Wennberg, P. O., Wisthaler, A., and Wolfe, G. M.: Airborne
812   measurements of western US wildfire emissions: Comparison with prescribed burning and air
813   quality implications, J. Geophys. Res.-Atmos., 122, 6108–6129, doi: 10.1002/2016JD026315,
814   2017.
815
816   Melvin, M. A.: 2015 National Prescribed Fire Use Survey Report, Technical Report, Coalition of
817   Prescribed Fire Councils, Inc. [online] Available from:
818   http://stateforesters.org/sites/default/files/publication-
819   documents/2015%20Prescribed%20Fire%20Use%20Survey%20Report.pdf, 2015.
820
821   Matt, F. J., Dietenberger, M. A. and Weise, D. R.: Summative and ultimate analysis of live
822   leaves from southern U.S. forest plants for use in fire modeling, Energy Fuels, (34), 4703–4720,
823   doi:10.1021/acs.energyfuels.9b04107, 2020.
824
825   Neuman, J. A., Huey, L. G., Ryerson, T. B., and Fahey, D. W.: Study of Inlet Materials for
826   Sampling Atmospheric Nitric Acid, Environ. Sci. Technol., 33, 1133-1136, doi:
827   10.1021/es980767f, 1999.
828
829   Paton-Walsh, C., Deutscher, N. M., Griffith, D. W. T., Forgan, B. W., Wilson, S. R., Jones, N.
830   B., and Edwards, D. P.: Trace gas emissions from savanna fires in northern Australia, J.
831   Geophys. Res., 115, doi:10.1029/2009JD013309, 2010.
832
833   Paton-Walsh, C., Smith, T. E. L., Young, E. L., Griffith, D. W. T. and Guérette, É.-A.: New
834   emission factors for Australian vegetation fires measured using open-path Fourier transform
835   infrared spectroscopy- Part 1: Methods and Australian temperate forest fires, Atmos. Chem.
836   Phys., 14, 11313-11333, doi: 10.5194/acp-14-11313-2014, 2014.
837
838   Phillips, M. C., Myers, T. L., Johnson, T. J., and Weise, D. R.: In-situ measurement of pyrolysis
839   and combustion gases from biomass burning using swept wavelength external cavity quantum
840   cascade lasers, Optics Express, 28(6), 8680-8700, 2020
841
842   Prior, R. L., Cao, G., Martin, A., Sofic, E., McEwen, J., O'Brien, C., Lischner, N., Ehlenfeldt,
843   M., Kalt, W., Krewer, G. and Mainland, C. M.: Antioxidant Capacity As Influenced by Total
844   Phenolic and Anthocyanin Content, Maturity, and Variety of Vaccinium Species, J. Agric. Food
845   Chem., 46(7), 2686–2693, doi:10.1021/jf980145d, 1998.

846   Pyne, S. J.: World fire: the culture of fire on earth, Pbk. ed., University of Washington Press,
847   Seattle., 1997.

848   Rao, P. V. R. and Rao, G. R.: Vibrational analysis of substituted phenols Part I. Vibrational
849   spectra, normal coordinate analysis and transferability of force constants of some formyl-,

850   methoxy-, formylmethoxy-, methyl- and halogeno-phenols, Spectrochimica ACTA Part A, 58,
851   3039-3065, 2002.

852   Roscioli, J. R., Zahniser, M. S., Nelson, D. D., Herndon, S. C., and Kolb, C. E.: New Approaches
853   to Measuring Sticky Molecules: Improvements of Instrumental Response Times Using Active
854   Passivation, J. Phys. Chem. A, 120, 1347-1357, doi: 10.1021/acs.jpca.5b04395, 2015.

855   Safdari, M.-S., Rahmati, M., Amini, E., Howarth, J. E., Berryhill, J. P., Dietenberger, M., Weise,
856   D. R., and Fletcher, T. H.: Characterization of pyrolysis products from fast pyrolysis of live and
857   dead vegetation native to the Southern United States, Fuel, 229, 151-166, 2018.

858   Safdari, M.-S., Amini, E., Weise, D. R. and Fletcher, T. H.: Comparison of pyrolysis of live
859   wildland fuels heated by radiation vs. convection, Fuel, 268, 117342,
860   doi:10.1016/j.fuel.2020.117342, 2020.

862   Saiz-Jimenez, C. and De Leeuw, J. W.: Lignin pyrolysis products: Their structures and their
863   significance as biomarkers, Organic Geochemistry, 10(4–6), 869–876, doi:10.1016/S0146-
864   6380(86)80024-9, 1986.

866   Scharko, N. K., Oeck, A. M., Myers, T. L., Tonkyn, R. G., Banach, C. A., Baker, S. P., Lincoln,
867   E. N., Chong, J., Corcoran, B. M., Burke, G. M., Ottmar, R. D., Restaino, J. C., Weise, D. R. and
868   Johnson, T. J.: Gas-phase pyrolysis products emitted by prescribed fires in pine forests with a
869   shrub understory in the southeastern United States, Atmos. Chem. Phys., 19(15), 9681–9698,
870   doi:10.5194/acp-19-9681-2019, 2019a.

871   Scharko, N. K., Oeck, A. M., Tonkyn, R. G., Baker, S. P., Lincoln, E. N., Chong, J., Corcoran,
872   B. M., Burke, G. M., Weise, D. R., Myers, T. L., Banach, C. A., Griffith, D. W. T. and Johnson,
873   T. J.: Identification of gas-phase pyrolysis products in a prescribed fire: first detections using
874   infrared spectroscopy for naphthalene, methyl nitrite, allene, acrolein and acetaldehyde,
875   Atmospheric Measurement Techniques, 12(1), 763–776, doi:10.5194/amt-12-763-2019, 2019b.

877   Scott, A. C., Bowman, D. M. J. S., Bond, W. J., Pyne, S. J. and Alexander, M. E.: Fire on earth:
878   an introduction, John Wiley & Sons, Inc, Chichester, West Sussex., 2014.

880   Sekimoto, K., Koss, A. R., Gilman, J. B., Selimovic, V., Coggon, M. M., Zarzana, K. J., Yuan,
881   B., Lerner, B. M., Brown, S. S., Warneke, C., Yokelson, R. J., Roberts, J. M., and de Gouw, J.:
882   High-and low-temperature pyrolysis profiles describe volatile organic compound emissions from
883   western US wildfire fuels, Atmospheric Chemistry & Physics, 18, 2018.

885   Selimovic, V., Yokelson, R. J., Warneke, C., Roberts, J. M., Gouw, J. d., Reardon, J., and
886   Griffith, D. W. T.: Aerosol optical properties and trace gas emissions by PAX and OP-FTIR for
887   laboratory-simulated western US wildfires during FIREX, Atmos. Chem. Phys., 18, 2929-2948,
888   2018.

890   Sharpe, S.W., Sams, R.L., Johnson, T.J., Chu, P.M., Rhoderick, G.C., and Guenther,
891   F.R.: Creation of 0.10-cm^{-1} resolution quantitative infrared spectral libraries for gas samples,

Atmospheric
Measurement
Techniques
Discussions

892   Proc. SPIE 4577, Vibrational Spectroscopy-based Sensor Systems, doi:
893   https://doi.org/10.1117/12.455730, 2002.
894

895   Shimanouchi, T.: Tables of Vibrational Frequencies, Consolidated Vol. I. National Bureau of
896   Standards, 1972.
897

898   Smith, T., Paton-Walsh, C. P., Meyer, G. C., Maier, S. W., Russell-Smith, J., Wooster, M., and
899   Yates, C. P.: New emission factors for Australian vegetation fires measured using open-path
900   Fourier transform infrared spectroscopy-Part: Australian tropical savanna fire, Atmos. Chem.
901   Phys. 14, 14, 11335–11352, 2014.
902

903   Smith, T., Clare Paton-Walsh, C. P. Meyer, Garry Cook, Stefan W. Maier, Jeremy Russell-
904   Smith, Martin Wooster, and Cameron P. Yates. "New emission factors for Australian vegetation
905   fires measured using open-path Fourier transform infrared spectroscopy-Part 2: Australian
906   tropical savanna fires." (2014): 11335.
907

908   Stein, Y. S., Antal Jr, M. J., and Jones Jr., M.: A study of the gas-phase pyrolysis of glycerol, J.
909   Anal. Appl. Pyrol., 4, 283–296, 1983.
910

911   Stockwell, C. E., Yokelson, R., Kreidenweis, S. M., Robinson, A. L., DeMott, P. J., Sullivan, R.
912   C., Reardon, J., Ryan, K. C., Griffith, D. W. T., and Stevens, L.: Trace gas emissions from
913   combustion of peat, crop residue, domestic biofuels, grasses, and other fuels: configuration and
914   Fourier transform infrared (FTIR) component of the fourth Fire Lab at Missoula Experiment
915   (FLAME-4), Atmos. Chem. Phys., 14, 9727-9754, 2014.
916

917   Susott, R. A.: Characterization of the thermal properties of forest fuels by combustible gas
918   analysis, For. Sci., 28(2), 404–420, 1982.

919   Thomas, S., Ledesma, E. B. and Wornat, M. J.: The effects of oxygen on the yields of the
920   thermal decomposition products of catechol under pyrolysis and fuel-rich oxidation conditions,
921   Fuel, 86(16), 2581–2595, doi:10.1016/j.fuel.2007.02.003, 2007.
922

923   Tihay, V. and Gillard, P.: Pyrolysis gases released during the thermal decomposition of three
924   Mediterranean species, Journal of Analytical and Applied Pyrolysis, 88(2), 168–174,
925   doi:10.1016/j.jaap.2010.04.002, 2010.
926

927   Varhegyi, G., Jakab, E. and Antal, M. J.: Is the Broido-Shafizadeh Model for Cellulose Pyrolysis
928   True?, Energy Fuels, 8(6), 1345–1352, doi:10.1021/ef00048a025, 1994.

929   Viatte, C., Strong, K., Hannigan, J., Nussbaumer, E., Emmons, L. K., Conway, S., Paton-Walsh,
930   C., Hartley, J., Benmergui, J. and Lin, J.: Identifying fire plumes in the Arctic with tropospheric
931   FTIR measurements and transport models, Atmos. Chem. Phys., 15, 2227-2246, doi:, 2015.

932   Waldrop, T. A. and Goodrick, S. L.: Introduction to prescribed fires in southern ecosystems,
933   Science Update, USDA Forest Service, Southern Research Station, Asheville, NC. [online]
934   Available from: http://www.treesearch.fs.fed.us/pubs/41316, 2012.

935   Ward, D. E. and Hao, W. M.: Projections of emissions from burning of biomass for use in
936   studies of global climate and atmospheric chemistry, 19 p., Air and Waste Management
937   Association, Vancouver, British Columbia, Canada. [online] Available from:
938   http://www.treesearch.fs.fed.us/pubs/43258, 1991.

939   Ward, D. E., and Hardy, C. C.: Smoke emissions from wildland fires, Environ. Int., 17, 117-134,
940   1991.

941   Ward, D. E. and Radke, L. F.: Emissions measurement from vegetation fires: a comparative
942   evaluation of methods and results, in Fire in the environment: the ecological, atmospheric, and
943   climatic importance of vegetation fires: report of the Dahlem Workshop, held in Berlin, 15-20
944   March 1992, edited by P. J. Crutzen and J. G. Goldammer, pp. 53–76, John Wiley & Sons Ltd.
945   [online] Available from: http://www.fs.fed.us/rm/pubs_other/rmrs_1993_ward_d001.pdf, 1993.

946   Ward, D. E.: Combustion chemistry and smoke, in Forest Fires: Behavior and Ecological Effects,
947   edited by E. A. Johnson and K. Miyanishi, pp. 55–77, Academic Press, San Diego, CA. [online]
948   Available from: http://www.doi.org/10.1016/B978-012386660-8/50006-3, 2001.

949   Warneke, C., Roberts, J. M., Veres, P., Gilman, J., Kuster, W. C., Burling, I., Yokelson, R., and
950   de Gouw, J. A.: VOC identification and inter-comparison from laboratory biomass burning using
951   PTR-MS and PIT-MS, Int. J. Mass Spectrom., 303, 6–14, doi:10.1016/j.ijms.2010.12.002, 2011.

952   Weise, D. R., Fletcher, T. H., Cole, W., Mahalingam, S., Zhou, X., Sun, L., and Li, J.: Fire
953   behavior in chaparral- Evaluating flame models with laboratory data, Combust. and Flame, 191,
954   500-512, https://doi.org/10.1016/j.combustflame.2018.02.012, 2018.

955   Weise, D. R., Johnson, T. J. and Reardon, J.: Particulate and trace gas emissions from prescribed
956   burns in southeastern U.S. fuel types: Summary of a 5-year project, Fire Safety Journal, 74, 71–
957   81, doi:10.1016/j.firesaf.2015.02.016, 2015.

958   Weise, D. R., Palarea-Albaladejo, J., Johnson, T. J., and Jung, H.: Analyzing Wildland Fire
959   Smoke Emissions Data Using Compositional Data Techniques, J. Geophys. Res. Atmos., 125(6),
960   https://doi.org/10.1029/2019JD032128, 2020.

961   Williams, S.D., Johnson, T.J., Sharpe, S.W., Yavelak, V., Oates, R.P. and Brauer, C.S.:
962   Quantitative vapor-phase IR intensities and DFT computations to predict absolute IR spectra
963   based on molecular structure: I. Alkanes. Journal of Quantitative Spectroscopy and Radiative
964   Transfer, 129, 298-307, https://doi.org/10.1016/j.jqsrt.2013.07.005, 2013

965   Yang, H., Yan, R., Chen, H., Lee, D. H. and Zheng, C.: Characteristics of hemicellulose,
966   cellulose and lignin pyrolysis, Fuel, 86, 1781–1788, 2007.

967   Yee, L. D., Kautzman, K. E., Loza, C. L., Schilling, K. A., Coggon, M. M., Chhabra, P. S.,
968   Chan, M. N., Chan, A. W. H., Hersey, S. P., Crounse, J. D., Wennberg, P. O., Flagan, R. C., and
969   Seinfeld, J. H.: Secondary organic aerosol formation from biomass burning intermediates: phenol
970   and methoxyphenols, Atmos. Chem. Phys., 13, 8019–8043, https://doi.org/10.5194/acp-13-8019-
971   2013, 2013.

Atmospheric
Measurement
Techniques
Discussions

Open Access

972 Yokelson, R. J., Griffith, D. W. T. and Ward, D. E.: Open-path Fourier transform infrared studies
973 of large-scale laboratory biomass fires, Journal of Geophysical Research, 101(D15), 21067,
974 doi:10.1029/96JD01800, 1996.

975 Yokelson, R. J., Susott, R., Ward, D. E., Reardon, J., and Griffith, D. W. T.: Emissions from
976 smoldering combustion of biomass measured by open-path Fourier transform infrared
977 spectroscopy, J. Geophys. Res. Atmos., 102, 18865-18877, 1997.

978 Yokelson, R. J., Christian, T. J., Bertschi, I. T., and Hao, W. M.: Evaluation of adsorption effects
979 on measurements of ammonia, acetic acid, and methanol, J. Geophys. Res., 108, 4649,
980 doi:10.1029/2003JD003549, 2003.

981 Yokelson, R. J., Burling, I. R., Gilman, J. B., Warneke, C., Stockwell, C. E., Gouw, J. d., Akagi,
982 S. K., Urbanski, S. P., Veres, P., Roberts, J. M., Kuster, W. C., Reardon, J., Griffith, D. W. T.,
983 Johnson, T. J., Hosseini, S., Miller, J. W., Cocker III, D. R., Jung, H., and Weise, D. R.:
984 Coupling field and laboratory measurements to estimate the emission factors of identified and
985 unidentified trace gases for prescribed fires, Atmos. Chem. Phys., 13, 89-116, 2013.

986 Zhou, X. and Mahalingam, S.: Evaluation of reduced mechanism for modeling combustion of
987 pyrolysis gas in wildland fire, Combustion Science and Technology, 171(1), 39–70,
988 doi:10.1080/00102200108907858, 2001.

989